REVIEW ARTICLE

An Observational History of the Direct Influence of the Stratospheric Quasi-biennial Oscillation on the Tropical and Subtropical Upper Troposphere and Lower Stratosphere

Matthew H. HITCHMAN

Department of Atmospheric and Oceanic Sciences, University of Wisconsin–Madison, Wisconsin, USA

Shigeo YODEN

Institute for Liberal Arts and Sciences and Graduate School of Science, Kyoto University, Kyoto, Japan

Peter H. HAYNES

Department of Applied Mathematics and Theoretical Physics, Cambridge University, United Kingdom

Vinay KUMAR

Radio and Atmospheric Physics Lab, Rajdhani College, University of Delhi, India

and

Susann TEGTMEIER

Department of Physics and Engineering Physics, University of Saskatchewan, Canada

(Manuscript received 4 May 2020, in final form 3 November 2020)

Abstract

The history of observational studies regarding the influence of the stratospheric quasi-biennial oscillation (QBO) on the tropical and subtropical upper troposphere and lower stratosphere (UTLS) is reviewed. QBO phases of westerly (QBO W) and easterly (QBO E) winds are defined in the lower stratosphere. During 1960–1978, radiosonde data revealed QBO modulation of the UTLS with a warm anomaly during QBO W in the tropics and cool anomalies near 30°S and 30°N. This pattern agreed with theory of the QBO mean meridional circulation (MMC), which predicted a coherent, antiphased response between the tropics and subtropics. During 1978–1994, satellite observations of aerosol and temperature confirmed the existence of the QBO MMC. During 1994–2001, global data sets enabled analysis of zonal mean QBO variations in tropopause temperature. In 2001, National Centers for Environmental Prediction reanalyses for the 42-yr period 1958–2000 revealed seasonal and geographical variations in QBO W–E tropopause temperature, pressure, and zonal wind, which are presented here. An update using the 38-yr Modern-Era Retrospective Analysis for Research and Applications, Version 2, and the 40-yr Euro-

Corresponding author: Matthew H. Hitchman, Department of Atmospheric and Oceanic Sciences, University of Wisconsin–Madison, 1225 West Dayton Street, Madison, Wisconsin, 53706, USA
E-mail: matt@aos.wisc.edu
J-stage Advance Published Date: 2 December 2020

pean Centre for Medium Range Weather Forecasts Reanalysis (ERA-Interim) data sets provides a more complete view of seasonal and geographical variation.

The QBO range in tropical tropopause values is ~ 0.5–2 K, ~ 100–300 m, and ~ 1–3 hPa, being colder and higher during QBO E, especially during boreal winter and spring. The QBO temperature signal tends to be larger near regions where deep convection is common. The QBO signal in the southern subtropics is enhanced during austral winter. During QBO W, the subtropical westerly jet is enhanced, while the Walker circulation is weaker, especially during boreal spring. A new climatology of the QBO MMC is presented. QBO E may enhance convection by reducing both static stability and wind shear in the UTLS.

Keywords quasi-biennial oscillation; tropopause; tropics; subtropics; general circulation

Citation Hitchman, M. H., S. Yoden, P. H. Haynes, V. Kumar, and S. Tegtmeier, 2021: An observational history of the direct influence of the stratospheric quasi-biennial oscillation on the tropical and subtropical upper troposphere and lower stratosphere. *J. Meteor. Soc. Japan*, **99**, 239–267, doi:10.2151/jmsj.2021-012.

1. Introduction

The westward progression of orange sunsets around the globe in the tropics after the eruption of Krakatau in August 1883 showed that there was a layer of easterly winds in the tropical stratosphere at that time (Simkin and Fiske 1984; Winchester 2003; Hamilton 2012). In August 1908, Berson (1910) found a thin layer of westerly winds in pilot balloon observations over tropical Africa, underlying a layer of easterly winds. This view of a layered structure, with "Krakatau easterlies" overlying a thin layer of "Berson westerlies", prevailed for fifty years (Hastenrath 2007; Brönniman and Stickler 2013), until several consecutive years of tropical radiosonde data were analyzed by Reed et al. (1961) and Veryard and Ebdon (1961). These papers reported the discovery of the stratospheric quasi-biennial oscillation (QBO), wherein alternating layers of QBO westerly winds (QBO W) and QBO easterly winds (QBO E) descend in the stratosphere at ~ 1 km month^{-1}, and diminish in amplitude approaching the upper troposphere/lower stratosphere (UTLS), exhibiting a variable periodicity of ~ 24–32 months (Fig. 1).

The QBO is primarily driven by vertical momentum fluxes due to upward-propagating equatorial wave activity, which are generated by tropospheric convective systems (Andrews et al. 1987). Another wave driving contribution comes from the meridional momentum flux convergence associated with extratropical planetary waves (Dunkerton 1983). Usually, this process is not as important as tropical wave driving, but it has been shown to be a likely cause for the disruption of descending QBO W during 2015/2016 (Osprey et al. 2016; Newman et al. 2016; Coy et al. 2017).

An overview of the QBO is provided by Baldwin et al. (2001). The focus of the present historical review is on observational studies of QBO effects in the UTLS in the tropics and subtropics, including the tropical tropopause layer (TTL). Gettelman and Forster (2002) suggested that the TTL extends from the level of lapse rate minimum at 10–12 km to the mean cold point tropopause (CPT) level at 17 km or 90 hPa. Fueglistaler et al. (2009) analyzed a range of meteorological and constituent data and suggested a working definition of the TTL as the 14–18.5 km layer (150–70 hPa or 355–425 K layer). Since the QBO mean meridional circulation (MMC) extends into the subtropics and upward into the stratosphere, the term UTLS will be used to indicate the tropical and subtropical upper troposphere and lower stratosphere.

Since the discovery of the QBO, observational studies have revealed interesting correlations between the QBO and other phenomena, including an antiphased relationship between the tropical and subtropical lower stratosphere (Angell and Korshover 1964) and modulation of the tropical tropopause altitude (Reid and Gage 1985). Evidence also emerged that the QBO influences the winter polar vortex, where QBO E favors a more disturbed polar vortex (Holton and Tan 1980). Anstey and Shepherd (2014) provide a comprehensive review of studies of the "Holton–Tan effect". Boville (1984), Baldwin and Dunkerton (1999), Thompson and Wallace (2001), and others have shown that the state of the extratropical stratosphere can modulate extratropical tropospheric weather patterns. This constitutes an extratropical stratosphere–troposphere coupling pathway, whereby the QBO can influence tropospheric weather via the extratropical stratosphere.

An evaluation of global reanalyses of the QBO signal in zonal wind is given by Kawatani et al. (2016).

A summary of global surface impacts of the QBO is given by Gray et al. (2018). Attard and Coy (2019) discuss QBO effects on the polar winter stratosphere. Haynes et al. (2021) provide an overview of theoretical and modeling aspects of the coupling between the stratosphere and troposphere involving the QBO, including a discussion of the interaction between the QBO and the Madden Julian Oscillation.

The present review focuses on the history of observationally based studies regarding the direct influence of the QBO on the tropical and subtropical UTLS. The primary purpose here is to describe significant relationships seen in the observations. An assessment of possible mechanisms, evaluated for consistency with the observed geographical distribution of the QBO signal in the UTLS, is given near the end. This history is described sequentially, according to stages of development in instrumental and global analysis capabilities. During 1960–1978, radiosonde data provided the first observations of QBO effects in the tropical and subtropical UTLS, with simultaneous development of a theoretical description of the QBO MMC as a wave-driven circulation. During 1978–1994, new satellite observations of volcanic aerosol and temperature provided information that supported the theoretical structure of the QBO MMC. During 1994–2001, development of global data sets allowed for new estimations of the zonal mean QBO in tropopause temperature, highlighting the latitudinal antiphased nature and effect across the UTLS.

In the early 2000s, data from the National Centers for Environmental Prediction (NCEP) for the period 1958–2000 were used by the lead author (MHH) to investigate the seasonal and geographical variation of the QBO signal in the tropical and subtropical UTLS. Results were presented orally at five international scientific meetings during 2000–2003, including the SPARC 2nd General Assembly, Mar del Plata, Argentina (November 6–10, 2000), the Japan–U.S. Seminar on Coupling of the Troposphere and Stratosphere by Dynamical, Radiative and Chemical Processes, Kyoto, Japan (March 13–17, 2001), the Risk Prediction Initiative Conference on Forecasting Severe Weather in Bermuda (2002), the AMS 12th Conference on Middle Atmosphere, San Antonio, USA (November 4–7, 2002), and the SPARC Workshop on the Role of the Stratosphere in Tropospheric Climate, Whistler BC, Canada (April 29–May 2, 2003). Three of these figures are included as historical Figs. 14–16 in this paper. At the time, the primary focus regarding QBO influences on the troposphere was on the Holton–Tan effect. Although the idea of a "direct effect" of the QBO on the tropical and subtropical UTLS had been discussed in the literature since the 1960s, in the early 2000s it was not yet widely accepted. Presentation of these figures eventually helped to generate interest in the possibility that there are geographical variations in the QBO signal in the tropics. During 2015–2019, the second author (SY) reinvigorated interest in the direct effect of the QBO on tropical convection by organizing a series of workshops in Japan. The lead author gave six presentations on this topic during 2015–2020.

Now it is possible to compare the geographical and seasonal variation in the QBO signal in the deep tropics in the 2001 NCEP study with results using CPT temperatures from Modern-Era Retrospective Analysis for Research and Applications, Version 2 (MERRA-2) data for the 38-yr period 1980–2017, and with results from European Centre for Medium Range Weather Forecasts (ECMWF) Reanalysis (ERA-Interim) data from the 40-yr period 1979–2018. These modern data sets extend the observational record by almost two decades. Further analysis of ERA-Interim data enables a more comprehensive description of the seasonal and geographical variations in the QBO signal in the tropical and subtropical UTLS, and provides a new depiction of the QBO anomalies in zonal wind, temperature, and MMC in the region 1000-1 hPa, 40°S–40°N.

Data and analysis methods for the NCEP, MERRA-2, and ERA-Interim data sets are described in Section 2, including discussion of QBO indices and statistical significance testing for each index. The historical development of observational evidence for a direct influence of the QBO on the tropical and subtropical UTLS, including radiosonde and zonal mean satellite data, is presented in Section 3. Section 4 shows the seasonal and geographical variation in tropopause temperature, tropopause pressure, and 70–150 hPa zonal wind shear in the 1958–2000 NCEP record for December–January–February (DJF) and June–July–August (JJA). Evidence is shown for an amplification of the QBO W–E signal near centers of deep convection, and effects on the subtropical westerly jet (SWJ). Results for 1958–1978 and 1979–2000 are shown separately for comparison.

Modern global data sets now include an extra 20 years of observations, increasing the statistical significance of the results. Section 5 discusses the distributions of QBO W–E MERRA-2 CPT temperature for all four seasons and for the record mean during 1980–2017 in the band 20°S–20°N. In section 6, analysis of ERA-Interim data from 1978–2018 provides a more

complete picture of the QBO signal in the UTLS, including effects on the Walker circulation, the SWJ, seasonal effects in the deep tropics, and a new depiction of the QBO MMC. Section 7 summarizes primary findings regarding zonal mean QBO influences, geographical variation, and seasonal variation in the tropics and subtropics, and discusses possible coupling mechanisms that are consistent with the observed geographical variation of enhancement in QBO W–E anomalies.

2. Data and analysis

2.1 NCEP 1958–2000

In 2001, a range of synoptic charts of QBO W–E differences were created using global reanalysis meteorological fields from NCEP (https://www.cdc.noaa.gov; Kalnay et al. 1996; Kistler et al. 2001). Monthly averages on a 2.5° grid were calculated from daily averages for the 43-yr period 1958–2000 (43 years) and for the two subperiods 1958–1977 (20 years) and 1978–2000 (23 years). Tropopause temperature and tropopause pressure were available as specially analyzed fields. NCEP tropopause levels were defined with the standard lapse rate definition. Tropical tropopause definitions and seasonal distributions in the tropics are discussed by Hoerling et al. (1991), Tuck et al. (1993), Highwood and Hoskins (1998), Hoinka (1998, 1999), Randel et al. (2000), and Zhou et al. (2001). Seidel et al. (2001) showed that the lapse-rate and CPT definitions yield very similar spatial patterns for climatological tropopause temperature. As will be shown, QBO temperature anomalies in the UTLS exceed 5 km in thickness. The lapse rate tropopause, the CPT, and the 100 hPa surface are less than ~ 1 km apart vertically in the tropics, which suggests that these minor differences in altitude for analyzing NCEP, MERRA-2, and ERA-Interim data should not strongly impact the resulting patterns of QBO W–E differences.

Prior to 1978, the tropical tropopause was ~ 3 K cooler than after 1978 in the NCEP record (Pawson and Fiorino 1999; Randel et al. 2000; Huesmann and Hitchman 2003). Due to averaging by phase of the QBO, this discontinuity does not affect results of QBO W–E differences. QBO W–E difference maps were created for 1958–2000 for each season. In order to test for robustness of results, the data were broken into the two periods of 1958–1978 and 1979–2000, the results of which are shown in Section 4.

Huesmann and Hitchman (2001) explored the relationship between the QBO W–E signal in NCEP tropopause temperature and a QBO index based on the zonal mean zonal wind shear between the paired levels 10–20, 20–30, 30–50, and 50–70 hPa. They found that the 50–70 hPa wind shear index yielded the most coherent QBO W–E signal in the tropical UTLS. Threshold shear values were chosen to be $\pm$ 1.5 m s^{-1} (20 hPa)$^{-1}$ for sorting into QBO W and E categories. Use of a wind shear index provides a clear expectation for the phase of QBO temperature, where W shear is vertically coincident with a warm anomaly. This physical expectation allows for the use of a one-tailed Student's *t*-test. If winds from only one level are used, the location of the thermal anomaly is less certain. While 50–70 hPa shear is highly correlated with 50 hPa wind, the method of determining phase by 50–70 hPa shear was selected to create the NCEP QBO W–E difference maps, which are shown below as Figs. 13–15.

During 1958–2000 there were ~ 18 QBO cycles, with 220 W, 187 E, and 109 intermediate months. QBO W–E difference maps were created for each season. Variables examined included tropopause temperature, tropopause pressure, 70–150 hPa wind difference, 150 hPa geopotential height, 150 hPa horizontal winds, and 150 hPa relative vorticity. Seasonal means and standard deviations for DJF, March–April–May (MAM), JJA, and September–October–November (SON) were calculated for QBO W and QBO E. Statistical significance was evaluated using a one-sided Student's *t*-test (assuming that a warm anomaly near the tropical TTL is associated with W shear). To evaluate statistical significance, one degree of freedom was assumed for each year (i.e., $N = 43$ for 1958–2000, 21 for 1958–978, and 22 for 1979–2000). For a 28-month sinusoidal oscillation, the autocorrelation as a function of monthly lag decreases from 1.0 to ~ 0.7 in 3.5 months, and becomes negative after 7 months (cf. Fig. 8 of Fraedrich et al. 1993). This suggests that choosing N equal to the number of years in a data record is somewhat too stringent, and choosing N equal to the number of months in a data record may be somewhat too lenient. The dependence of the *p*-value on N for a given *t*-score is weak, such that an outcome of 95 % significance for $N = 20$ increases only to ~ 96 % for $N = 240$. For Figs. 14–16, N was chosen to be the number of years in the record, with light shading indicating confidence levels above 90 %, dark shading above 95 %, in a one-tailed Student's *t*-test.

2.2 MERRA-2 1980–2017

Cold-point tropopause temperatures from MERRA-2 were used for the 38-yr period 1980–2017. Values

were interpolated to the CPT using a cubic spline. The phase of the QBO was determined for this analysis using zonal winds at 50 hPa. Zonal wind at 50 hPa is highly correlated with 50–70 hPa zonal wind shear, so the two methods should yield similar results. The range in QBO temperature was defined to be the difference between the warmest and coldest monthly average for each QBO cycle at each location, averaged over all of the cycles during the 38-yr data record (456 total months). Statistical significance was determined by using a two-tailed Student's *t*-test and bootstrapping technique. Each month was assumed to be statistically independent, so that $N = 456$. Results are shown for QBO range in CPT temperature averaged for the total record and for each season in the deep tropics (20°S–20°N). In Fig. 17, regions with less than 99 % statistical significance are shown in black.

2.3 ERA-Interim 1979–2018

The ERA-Interim data assimilation system includes 4D variational analysis with a 12-hr window (Berrisford et al. 2011; Dee et al. 2011). The resolution of the data set is ~ 80 km (T255 spectral resolution), with 60 pressure levels from the surface to 0.1 hPa. Daily data from the 40-yr period of January 1, 1979–December 31, 2018 were used to create monthly-averaged values of temperature and the three wind components on pressure surfaces.

The phase of the QBO was determined by using the method of Wallace et al. (1993), which projects equatorial zonal wind profiles onto two empirical orthogonal functions (EOFs) in the vertical domain 70–10 hPa, to represent the vertical structure for each phase of the QBO. The first two principal components, PC1 and PC2, were defined by EOF analysis based on the covariance matrix of equatorial zonal-mean zonal wind at the five pressure levels 70, 50, 30, 20, and 10 hPa. The annual cycle was first removed by subtracting the 40-yr monthly mean climatology. EOF analysis was performed over the 40-yr ERA-Interim record. When QBO phase is plotted as a function of PC1 and PC2, which vary in time as the QBO descends, the trajectory maps out circles. Eight QBO phases are defined by averaging in 45° angular bins in PC1/PC2 space, where phase-1 is 0–45°, phase-2 is 45–90°, phase-3 is 90–135°, phase-4 is 135–180°, phase-5 is 180–225°, phase-6 is 225–270°, phase-7 is 270–315°, and phase-8 is 315–360°. Phase-4 and phase-8 correspond to when QBO W and QBO E, respectively, maximize in the lower stratosphere. In the current analysis, all the figures are based on phase-4 minus phase-8. This index corresponds closely to the 50–70 hPa index used for NCEP data and the 50 hPa zonal wind index used for MERRA2 data. Please see Fig. 3 and Section 3 in Wallace et al. (1993) and Fraedrich et al. (1993) for further details.

In order to provide a reference frame for the location of QBO anomalies in the UTLS, tropopause pressure was calculated for seasonal means (Fig. 20) and for the record average (Fig. 21). ERA-Interim temperature values were interpolated with a cubic spline to a 1-hPa vertical grid, the traditional lapse rate tropopause pressure was calculated, and then averaged by zonal mean and by season and data record.

In consideration of possible effects due to the El Niño Southern Oscillation (ENSO), a second data set was generated that only includes ENSO-neutral months (374 months). A neutral ENSO is defined to occur when the sea surface temperature anomaly from the monthly climatology (40 years) in the Niño3.4 region is between −1.0 K and 1.0 K. The sea surface temperature data set was obtained from the Hadley Centre Global Sea Ice and Sea Surface Temperature archive. Although results are almost identical for the two data sets, results are shown only for the ENSO-neutral data set.

Statistical significance is calculated by assuming two independent samples, one containing all of the months of phase-4 and another containing all the months for phase-8. The statistical significance test assumes that data for each month is independent from each other, which is the same assumption as that made for the MERRA2 data. The number of degrees of freedom assumed was 374. In Figs. 18–21, values which are less than 95 % statistically significant are indicated with diagonal green hatching.

Since seasonal averages are taken, and the QBO has a high autocorrelation for lags of ± 3 months or less, possible differences of ± 1–2 months that may result from the three different methods of identifying the phase should not severely affect the results. The overall similarity of results from the three analyses suggests that small differences in lag are not important.

3. Observational evidence of a direct influence of the QBO on the UTLS

3.1 1960–1978: radiosonde analysis and theory of the QBO MMC

In the 1960s, progress was made in diagnosing the theoretical structure of the QBO, while observational studies revealed interesting aspects about the QBO, including the degree of downward penetration of QBO wind regimes into the UTLS, the antiphased relation-

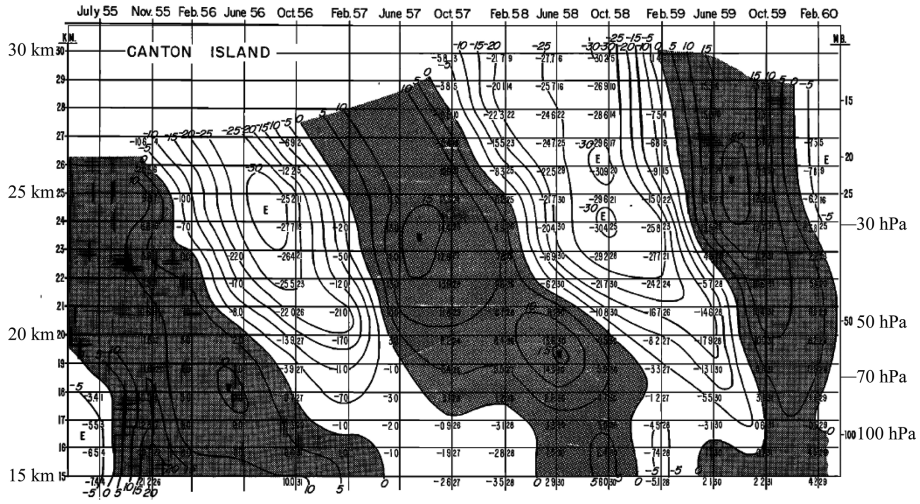

Fig. 1. Time–altitude section of monthly mean zonal wind (contour interval 5 m s^{-1}) at Canton Island (3°S, 172°W) in the altitude layer 15–30 km during the period March 1955–March 1960. Layer-averaged wind speeds (in m s^{-1}, with a space instead of a decimal point) are plotted to the left of vertical lines, while the number of observations in each mean is shown to the right (after Fig. 1 of Reed et al. 1961).

ship between the tropical and subtropical UTLS, and influences on the TTL. Figure 1 from Reed et al. (1961) shows the variation in zonal wind at Canton Island (3°S, 172°W) during the 5 years March 1955–March 1960. Features of note include the variable periodicity in the range ~22–34 months and variation in shape with altitude. Aspects that contribute to these variations include a more rapid descent rate for QBO W than QBO E, the existence of time mean easterlies in the middle stratosphere and time mean westerlies in the lower stratosphere, a seasonal modulation of descent rate (e.g., Dunkerton 2017), and seasonal and interannual variability in wave driving.

Note the significant QBO variation in vertical shear of the zonal wind, $\frac{\partial u}{\partial z}$, in the UTLS seen in Fig. 1. This includes the tropical TTL, into which deep convection penetrates to varying degrees (e.g., Folkins et al. 1999; Gettelman and Forster 2002; Gettelman et al. 2002; Dessler et al. 2006; Fueglistaler et al. 2009; Virts et al. 2010; Match and Fueglistaler 2019). Since the tropopause at Canton Island is near 17 km, Fig. 1 suggests that QBO wind regimes mildly influence the tropical upper troposphere. Note also that the sign of 30 hPa zonal wind is often different from the sign of 50–70 hPa wind shear, so it is more useful to use a lower stratospheric QBO index in assessing a "direct effect" on the tropical and subtropical UTLS.

The variation of 50 hPa temperature during 1957–1962 for radiosonde stations at a range of latitudes is shown in Fig. 2 (Angell and Korshover 1964), where the annual cycle has been removed with a 12-month running mean. Note the QBO signal at Canton (3°S), with a temperature range of ~3 K. Note that QBO temperatures in the subtropics tend to be out of phase with the tropics at 50 hPa in the Southern Hemisphere (SH) during this period. Tucker and Hopwood (1968, their Fig. 3) reported a strong QBO signal and covariation of zonal wind at Darwin (12°S) and Hobart (43°S) at 28 km altitude for the period 1960–1966. Angell and Korshover (1970, 1974), Wallace (1973), and Newell et al. (1974, Chapter 10) further documented QBO signals in tropical and extratropical lower stratospheric radiosonde temperatures.

Theoretical considerations of the QBO by Reed (1966), Wallace (1967), and Dickinson (1968) led to the realization that a zonal mean QBO MMC must exist to maintain the observed relationship between zonal wind and temperature, which is closely approximated by thermal wind balance. Figure 3a shows a schematic diagram of the theoretical QBO structure in temperature and meridional circulation from Dickinson (1968). A warm anomaly centered at the equator should exist below the maximum of QBO W, so that $\frac{\partial u}{\partial z} \propto -f\frac{\partial \theta}{\partial y} > 0$, and a cold anomaly should exist below the QBO E maximum, so that $\frac{\partial u}{\partial z} < 0$, to main-

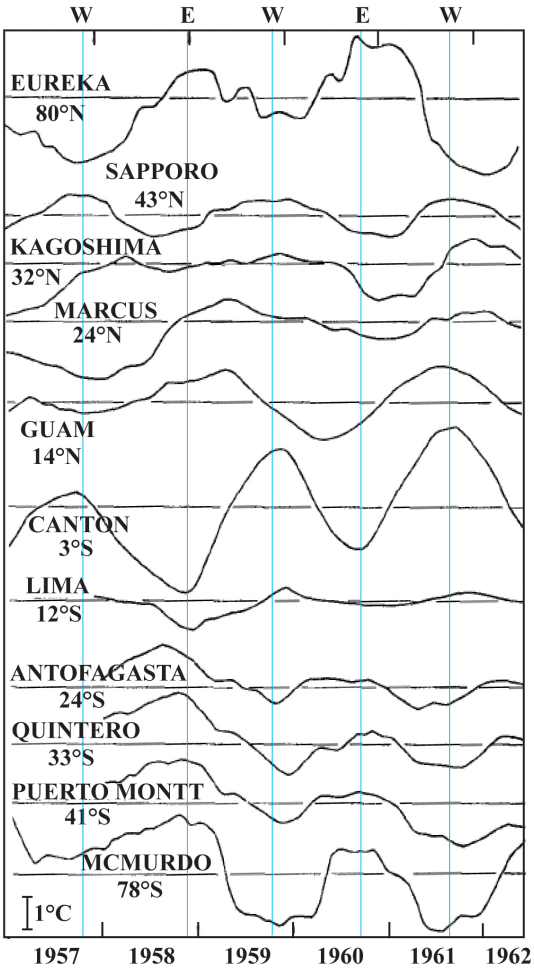

Fig. 2. Twelve-month running average of monthly mean 50 hPa temperatures for stations approximately evenly spaced north and south of the equator, in the range 80°N–76°S, during 1957–1962. The scale for 1°C is shown in the lower left inset. Short vertical tick marks correspond to the beginning of a year. Thin blue vertical lines were added to indicate QBO temperature extrema at Canton Island (after Fig. 3 of Angell and Korshover 1964).

tain temperature anomalies against radiative relaxation. This requires subsidence below the W maximum and ascent below the E maximum. This, in turn, implies the existence of a return circulation with opposing vertical motion in the subtropics. The anticorrelation between vertical motion and temperature is expected from a wave-driven circulation. Subsequent versions of this schematic diagram are found in Plumb and Bell (1982), reproduced here as Fig. 3b, and in Gray et al. (1992b), Trepte (1993), and Collimore et al. (2003).

Figure 3b reproduces the QBO MMC diagram from Plumb and Bell's (1982) iconic numerical modeling experiments, in which they generated a QBO by parameterized equatorial wave drag in the zonal momentum equation. Their diagram also suggests that the return circulation of the MMC extends outside of the tropics (Fig. 3b). However, observations at the time were as yet insufficient to determine the actual distribution and magnitude of the QBO MMC. A new depiction of the meridional structure of the QBO based on ERA-Interim analyses is shown as a summary diagram at the end of this review (Fig. 21).

The extent and similarity of QBO variations in tropopause height throughout Micronesia was described by Reid and Gage (1985). Figure 4 shows that variations in tropopause height with a range of ~ 200–300 m occurred at time scales of 22–34 months during the period of 1952–1982. These stations were all in the deep tropics and QBO variations were in phase.

Yasunari (1989) showed that there is an interesting coherence between Singapore zonal winds at 50 and 700 hPa at QBO periods (Fig. 5), where anomalous westerly flow at 700 hPa tends to occur when QBO W are present at 50 hPa. The power in the QBO band at 700 hPa (and at 200 hPa) is ~ 1/20 that at 50 hPa, so that QBO wind anomalies of 10 m s^{-1} at 50 hPa correspond to wind anomalies of perhaps 2 m s^{-1} at 700 hPa. Yasunari (1989) showed that QBO wind anomalies at 700 hPa are anticorrelated with 250 hPa winds, and argued that the Walker circulation tends to be stronger during QBO E. This would be consistent with strengthened tropical deep convection over Indonesia during QBO E. A study by Knaff (1993) found similar QBO influences on tropical tropospheric winds. It will be shown in Section 6 that analysis of ERA-Interim data supports Yasunari's (1989) idea that the Walker circulation tends to be weaker during QBO W.

3.2 1978–1994: Satellite observations of stratospheric temperature and aerosol

The launch of limb-scanning instruments on board polar-orbiting satellites in the late 1970s afforded an unprecedented view of stratospheric temperature and volcanic aerosol, including the limb infrared monitor of the stratosphere (LIMS) instrument (Gille and Russell 1984), which measured temperature, the Stratospheric Aerosol and Gas Experiment (SAGE I and II) instruments (McCormick et at. 1989), which sampled aerosol in the tropics and midlatitudes, and the Stratospheric Aerosol Measurement (SAM II) in-

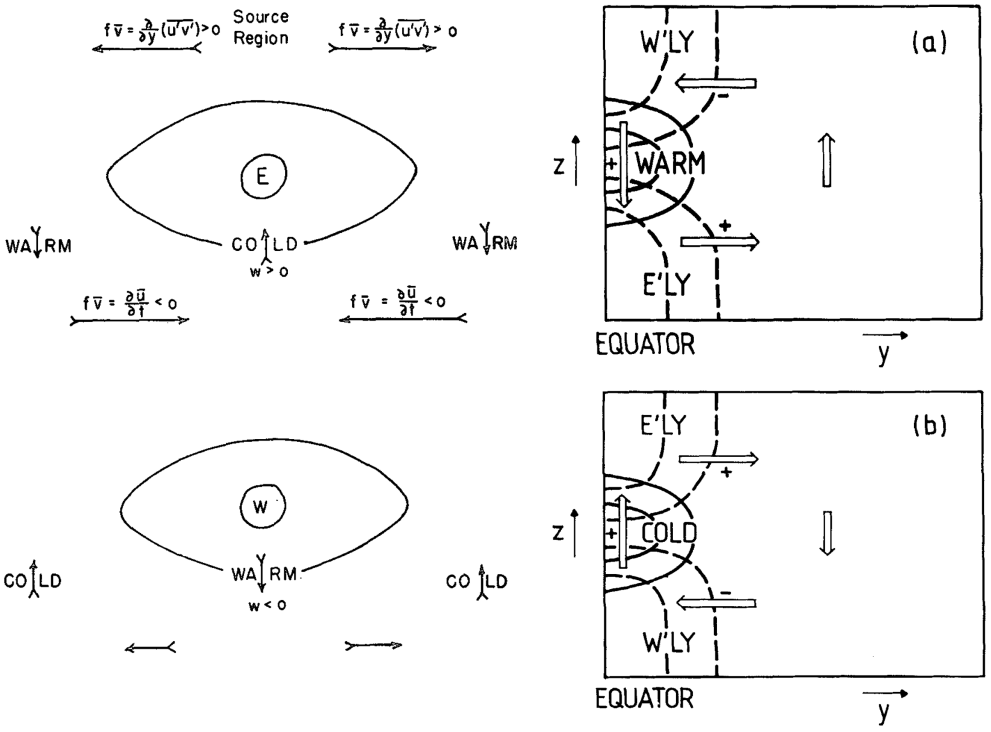

Fig. 3. Left (Fig. 3 of Dickinson 1968): "Schematic depiction of the kinematics of the theoretical downward progression of a biennial wave centered at the equator, showing easterlies overlying westerlies". The nature of the momentum forcing was not yet clear. Right (Fig. 1 of Plumb and Bell 1982): "Schematic representation of the mean meridional circulation driven by an equatorial thermal anomaly, and the consequent acceleration of the mean zonal wind [in part, after Reed (1964) and Dickinson (1968)]. Solid contours: potential isotherms. Dashed contours: isopleths of zonal velocity. +/−: sign of zonal acceleration. (a) Warm anomaly (b) Cold anomaly". In their 2D model, the circulation is obtained by parameterizing the absorption of eastward- and westward-travelling equatorial waves in the zonal momentum equation. Note the antiphasing of temperature anomalies in the subtropics and tropics implied by the MMC.

strument (Russell et al. 1981), which observed aerosol in the polar regions.

In diagnosing the distribution of zonal mean temperature, zonal wind, and absolute vorticity in LIMS data, Hitchman and Leovy (1986) argued that the QBO MMC modulates the distribution of temperature and absolute vorticity. Figure 6 shows zonal mean sections of these variables for the period October 31–November 5, 1978, when QBO westerlies were in the lowest stratosphere and QBO E were centered near 10 hPa (Fig. 6b). In Fig. 6c, normalized absolute vorticity is plotted: $\frac{f}{|f|}\left(f-\frac{\partial \bar{u}}{\partial y}\right)$, such that negative regions indicate anomalous absolute vorticity for a given hemisphere. The zero-wind line near 10 hPa separates QBO E below from QBO W above (Fig. 6b). Near 10 hPa, the temperature contours are pinched together over the equator and spread out vertically in the subtropics, consistent with the MMC indicated by the arrows in Fig. 6a. The distribution of absolute vorticity in Fig. 6c is also consistent with redistribution by the QBO MMC, where contours are spread apart just above the level of the QBO E wind maximum at ~ 10 hPa, with enhanced gradients in the subtropics near 25°S and 25°N. Near 50 hPa, contours appear pinched together towards the equator by a convergent flow (Fig. 6c). These results support the idea that the QBO MMC can affect the extratropics.

Trepte and Hitchman (1992) and Hitchman et al. (1994) used SAGE I and II and SAM II aerosol data to study the structure of the QBO. Fall velocities in the lower stratosphere for aerosol droplets ~ 0.1–1 μm in diameter are on the order of 0.1–0.5 mm s^{-1}. Since this is comparable to theoretical estimates of the

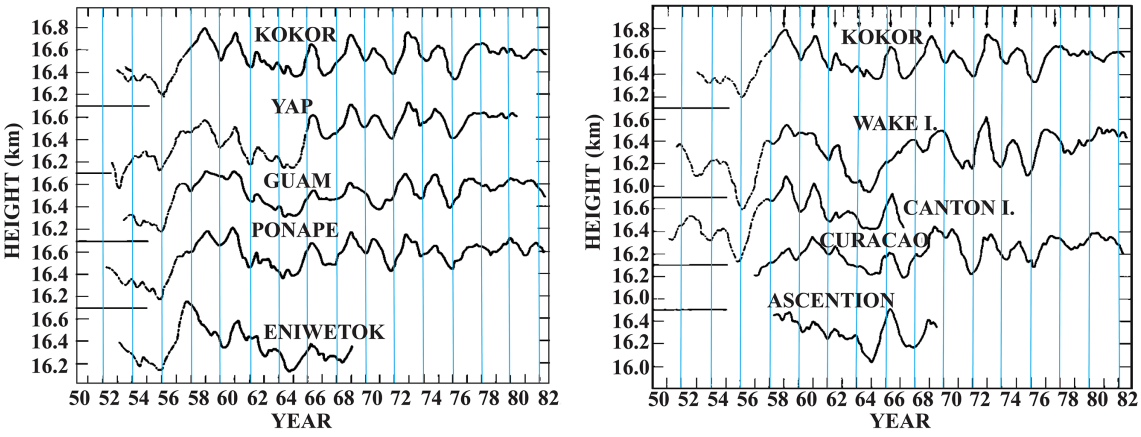

Fig. 4. Twelve-month running mean tropopause heights at five Micronesian stations (left panel, after Fig. 2 of Reid and Gage 1985) and for more widely separated stations, including Curacao and Ascension Island in the Atlantic (right panel, after Fig. 3 of Reid and Gage 1985), where arrows at the top identify peaks that occur at more than one station. The 16-km level is indicated for each curve at left. Thin blue vertical lines were added at the beginning of each even year.

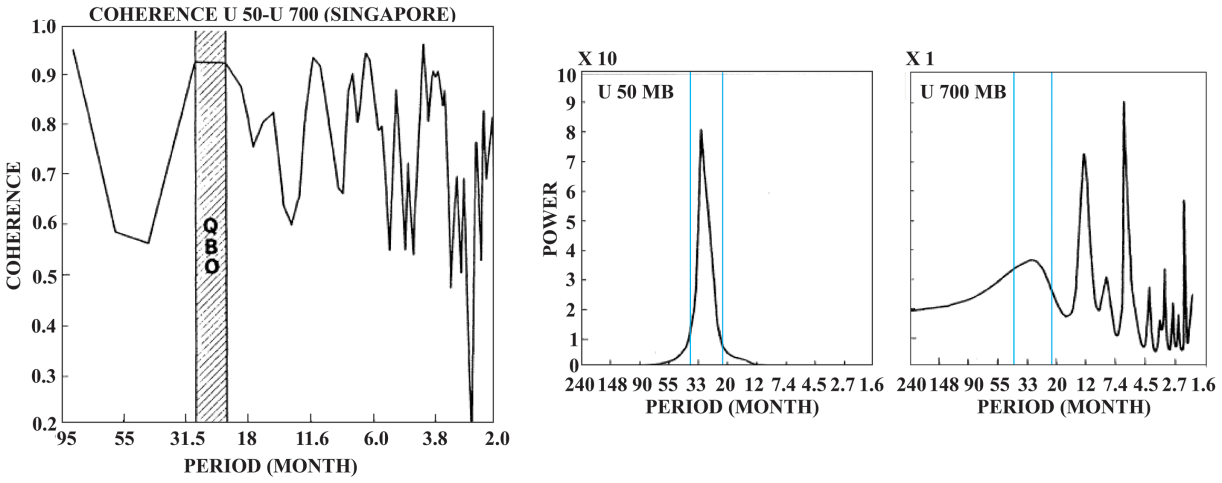

Fig. 5. Left: coherence spectrum of monthly mean zonal wind between 50 hPa and 700 hPa at Singapore. Right: individual power spectra at 50 hPa and 700 hPa for the 18-yr period 1963–1981. Power spectrum units plotted are in m s^{-1} per month and a maximum lag of 40 was used. Note that the power scale for 50 hPa is 10 times that for 700 hPa. Thin blue vertical lines were added to the power spectra to highlight the band ~ 22–36 months (adapted from Fig. 3 of Yasunari 1989).

magnitude of vertical motion associated with the QBO MMC, the distribution of volcanic aerosol can act as a "dye" to reveal the structure of the QBO MMC. Trepte and Hitchman (1992) showed sample 40-day "snapshots" of aerosol distributions in latitude–altitude which highlighted the QBO MMC. During QBO W (Fig. 7a), characteristic "horns" may be seen above the W maximum, compatible with sinking over the equator and rising motion in the subtropics. During QBO E (Fig. 7b), air is gathered and lofted over the equator, creating a narrower, taller vault of high aerosol concentrations.

Hitchman et al. (1994) showed that the QBO modulates the tropical aerosol reservoir, such that during QBO W, optical depth is reduced in the tropics and enhanced in the subtropics. Figure 8 shows QBO W–E

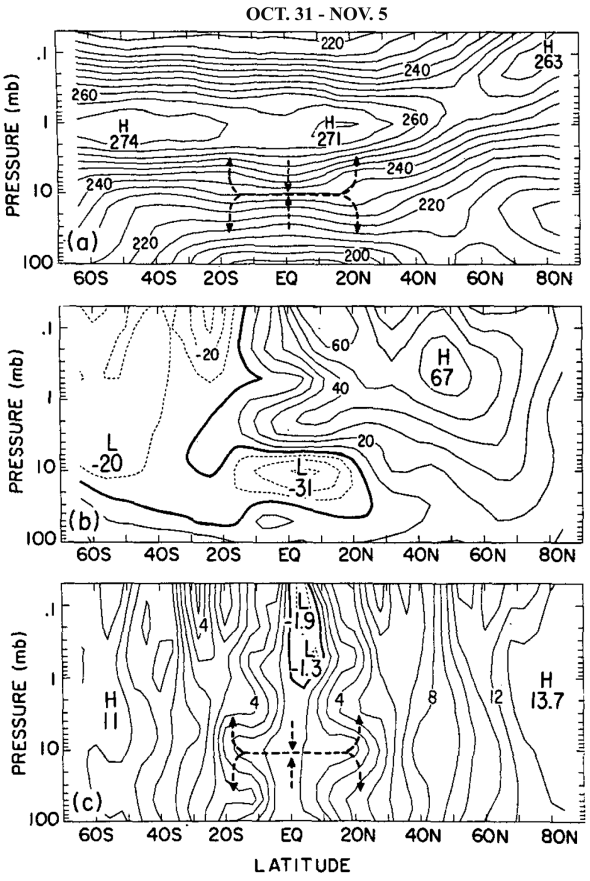

Fig. 6. Latitude–altitude sections of zonal mean LIMS a) temperature (contour interval, 5 K), b) zonal wind (interval, 10 m s^{-1}), and c) normalized absolute vorticity (see text, contour interval, 1 day^{-1}) for the period of October 31–November 5, 1978. Values of temperature and zonal wind have been smoothed with a 1-2-1 filter in latitude. Schematic arrows indicate the MMC that is compatible with the observed patterns in temperature and potential vorticity and with theoretical models (Fig. 4 of Hitchman and Leovy 1986, © American Meteorological Society, used with permission).

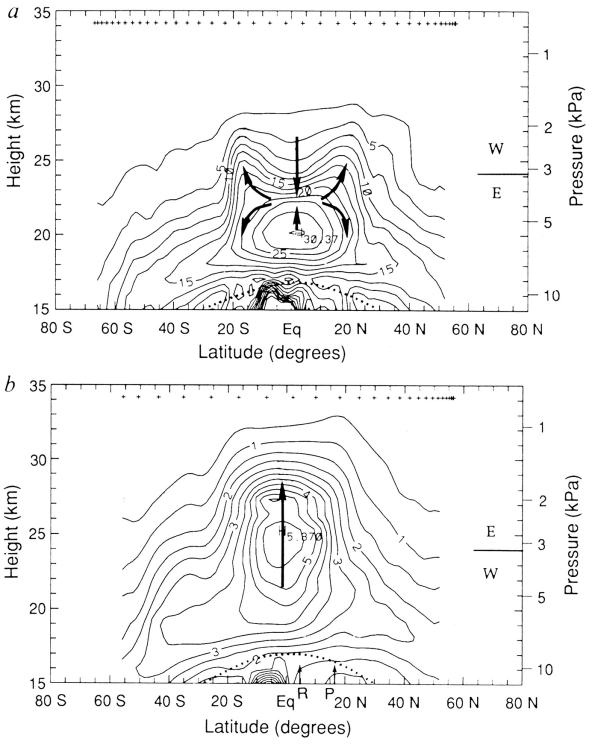

Fig. 7. Latitude–altitude sections of aerosol extinction ratio at 1 μm during two 40-day periods representative of two different phases of the QBO: a) dominant westerly shear centered at November 11, 1984 (contour interval, 2.5) and b) dominant easterly shear, centered at October 4, 1988 (contour interval, 0.5). Crosses indicate locations of the daily average of ~ 15 profiles. Arrows indicate the inferred QBO circulation based on the aerosol distribution. The tropopause is indicated with a dotted line. The latitudes for the eruptions of Mt. Ruiz in November 1985 and of Mt. Pinatubo in June 1991 are indicated by "R" and "P", respectively, both of which occurred during easterly shear in the lower stratosphere. The altitude of the zero-wind line at the equator is shown at the right of each section (Fig. 3 of Trepte and Hitchman 1992).

difference in aerosol extinction ratio values based on 10 years of data, with differences on the order of 20–50 %. During QBO W, descent occurs over the equator, with enhanced poleward motion and rising in the subtropics, spreading volcanic aerosol from the "tropical reservoir" into the extratropical lower stratosphere in a "lower transport regime" (Hitchman et al. 1994). During QBO E, aerosol is gathered and lofted in the tropical reservoir. Choi et al. (2002) analyzed the QBO influence on trace constituents from the Halogen Occultation Experiment. They also found a strong modulation of tracer distributions by the QBO MMC.

Figure 9 shows a schematic diagram of the effects of the QBO MMC on temperature and tropopause altitude, taken from Collimore et al. (2003). It is similar to figures in Gray et al. (1992b) and Trepte (1993). During QBO W (Fig. 9a), absorption of waves with

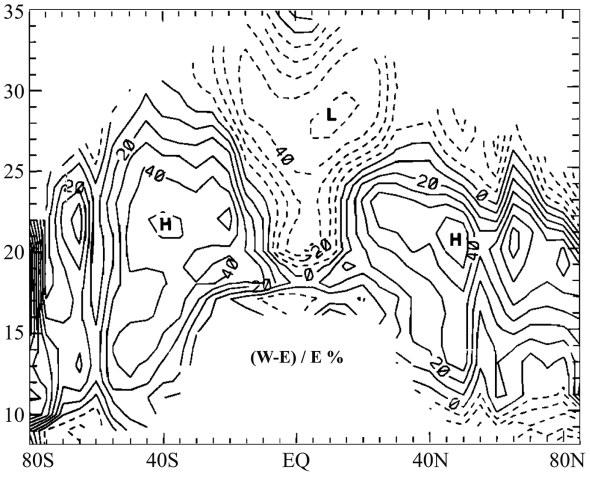

Fig. 8. QBO W–E differences in SAGE aerosol extinction ratio (contour interval, 5 %), using the 50–70 hPa wind shear index, based on 10 years (1979–1981 and 1984–1990) of SAGE I and II and SAM II aerosol measurements. Dashed contours indicate higher aerosol during QBO E shear (Fig. 7 of Hitchman et al. 1994).

westerly phase speeds causes westerly acceleration and convergent, equatorward flow, which imports lower angular momentum air from higher latitudes (Lindzen and Holton 1968). Mass convergence implies subsidence warming in the tropics and cooling by ascent in the flanking subtropics, with the resulting temperature anomalies yielding a consequent displacement of the tropopause downward in the tropics and upward in the subtropics. During QBO E (Fig. 9b), easterly wave drag causes easterly acceleration and poleward divergence. This requires ascent in the tropics and descent in the subtropics, with an upward deformation of the tropopause in the tropics and downward in the subtropics. A new climatology of the QBO MMC will be shown in Figs. 20 and 21.

In addition to QBO effects on the UTLS, other studies have found relationships between the QBO and tropical weather phenomena. Angell et al. (1969) suggested that Atlantic hurricanes are more plentiful during QBO W. Gray (1984) and Gray et al. (1992b) also found that the QBO influences Atlantic hurricane frequency, with QBO W favoring more hurricanes. They suggested that stronger westerly shear in the subtropical North Atlantic UTLS associated with QBO W reduces the local climatological easterly wind shear across the UTLS, thereby fostering growth of tropical cyclones. Gray and Schaeffer (1991) found evidence for QBO modulation of tropical cyclones in other ocean basins. Ho et al. (2009) showed that the QBO modulates the preferred longitude band of tropical cyclones in the western Pacific. However, Camargo and Sobel (2010) showed that the correlation between tropical cyclones and the QBO depends on the period of observation. Further observational study over a longer time may be required to understand this problem.

QBO effects on tropical rainfall have been reported by Hastenrath (1990), Gray et al. (1992a), and Kane (1995). In a study of outgoing longwave radiation (OLR) over Indonesia, Knaff (1993) showed that deep convection tends to be stronger, as seen in reduced OLR emitted from colder cloud tops, when QBO E shear is in the tropical UTLS. Collimore et al. (1998)

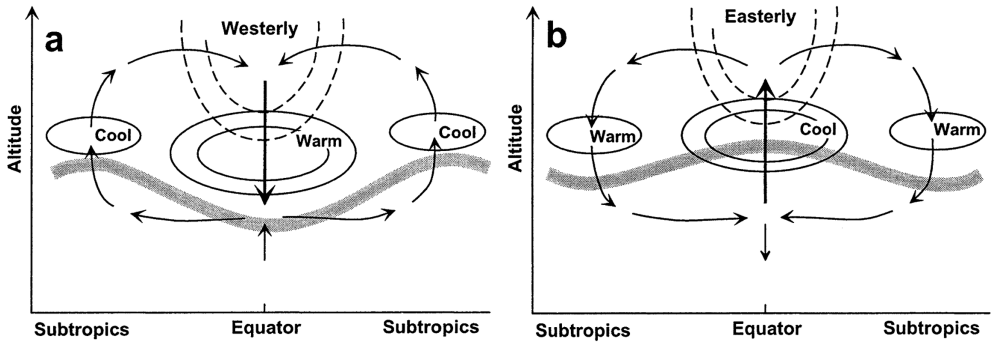

Fig. 9. Schematic diagram of the QBO MMC and its relationship with anomalies of zonal mean temperature (solid contours), zonal velocity (dashed contours), and tropopause altitude (thick gray lines) for a) warm anomaly during descending QBO W regime and b) cold anomaly during descending QBO E regime approaching the UTLS (from Collimore et al. 2003, © American Meteorological Society, used with permission. Cf. similar diagrams in Gray et al. 1991b and Trepte 1993).

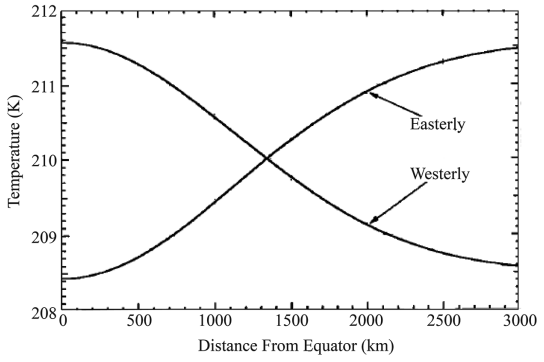

Fig. 10. "Calculated temperature anomalies forced by the easterly and westerly phases of the quasi-biennial wind variation". A typical value for vertical shear of 3 m s^{-1} per 6 km and a mean equatorial temperature of 210 K were assumed (Fig. 8 from Reid 1994).

showed that QBO E in the lower stratosphere favors more extensive deep convection in the three primary centers of chronic convection, Amazonia, Africa, and Indonesia, with effects being most notable during boreal winter.

3.3 1994–2000: QBO effect on the zonal mean UTLS in global analyses

The first attempt to make a quantitative estimate of the latitudinal structure of the QBO in temperature in the lower stratosphere was made by Reid (1994), who calculated temperature anomalies based on observed QBO variations in zonal wind, from the thermal wind law applied in the vicinity of the equator:

$$\frac{\partial T}{\partial y} = -\frac{2\Omega T y}{gR}\frac{\partial u}{\partial z}, \tag{1}$$

where u, T, and y are zonal wind, temperature, and latitude in meters, respectively, while Ω, g, and R are the earth's rotational angular velocity, gravitational acceleration, and radius, respectively. Assuming a typical value for shear of 3 m s^{-1} per 6 km and a mean equatorial temperature of 210 K, he estimated that, during QBO W, temperatures would be ~ 3 K warmer over the equator and ~ 3 K cooler near 30°S and 30°N compared to during QBO E (Fig. 10). This estimated range of 3 K turns out to be somewhat higher than in the results shown in Sections 4–6.

Randel et al. (1999) used stratospheric analyses from the United Kingdom Meteorological Service to estimate vertical velocities associated with the QBO MMC, by assuming that vertical advection balances

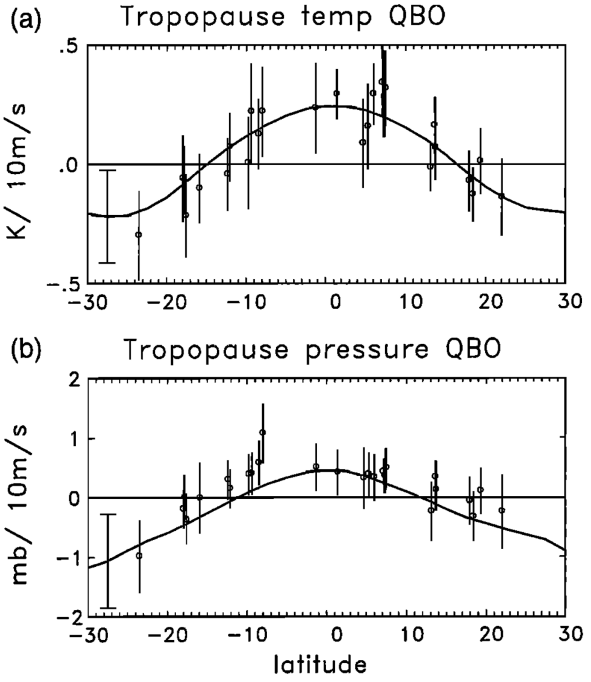

Fig. 11. "Latitudinal structure of QBO variations in a) tropopause temperature (K per 10 m s^{-1}) and b) tropopause pressure (hPa per 10 m s^{-1}) for 1979–1997, derived from regression analysis. Curves show NCEP data and circles indicate results for each radiosonde location. Error bars indicate ± 2 sigma statistical uncertainties. Units are Kelvins per 10 m s^{-1} of QBO winds at 50 hPa, which vary over ~ ± 20 m s^{-1} during a QBO cycle" (Fig. 13 of Randel et al. 2000).

radiative heating/cooling associated with a QBO temperature anomaly. They found upward motion in cold anomalies, with estimated QBO vertical motion magnitudes of less than 0.1 mm s^{-1} below 30 hPa (cf. their Fig. 13).

Randel et al. (2000) investigated interannual variability of the tropical tropopause derived from radiosonde data and NCEP reanalyses. They found "a strong signature of the QBO in tropopause statistics" that is primarily zonal mean in character. Using regression analysis on zonal winds for the period of 1979–1997, they estimated the latitudinal variation of tropopause temperature and tropopause pressure associated with the QBO (Fig. 11). They confirmed the antiphased nature of the signal in the tropics and subtropics, and estimated a range of ~ 1 K in tropical tropopause temperature and ~ 2 hPa in tropical tropopause pressure, assuming a range of 40 m s^{-1} for the

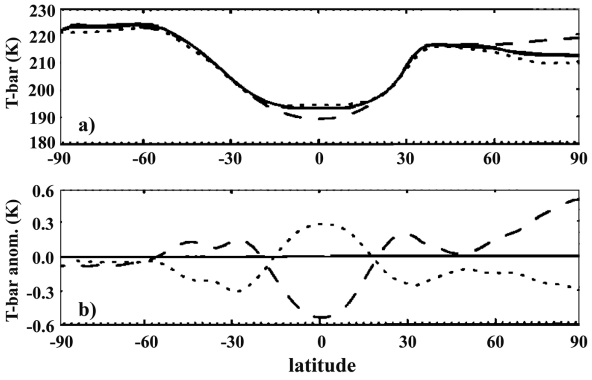

Fig. 12. a) Latitudinal distribution of NCEP zonal mean tropopause temperature (K) for DJF QBO W (dotted line), QBO E (dashed line), and climatological mean (solid line). b) QBO W (dotted line) and QBO E (dashed line) departure from the annually averaged zonal mean tropopause temperature (K). Deviations from climatology in a) are exaggerated by a factor of 5 for clarity (Fig. 15 of Huesmann and Hitchman 2001).

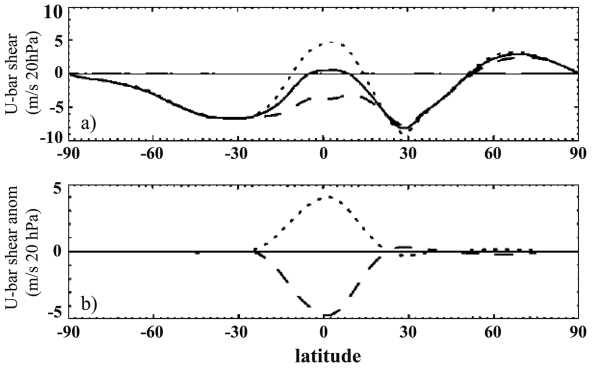

Fig. 13. a) Latitudinal distribution of NCEP 50–70 hPa zonal mean wind shear (m s^{-1} per 20 hPa) for DJF QBO W (dotted line), QBO E (dashed line), and climatological mean (solid line). b) QBO W (dotted line) and QBO E (dashed line) departure from the annually averaged 50–70 hPa wind shear (Fig. 9 of Huesmann and Hitchman 2001).

QBO in zonal wind.

Huesmann and Hitchman (2001) analyzed QBO variations in NCEP tropopause temperature, tropopause pressure, and zonal winds in the UTLS for the period 1978–2000. Figure 12a shows the zonal mean distribution of tropopause temperature for DJF. Figure 12b shows latitudinal profiles of QBO W and E anomalies. This shows a QBO range in zonal mean tropical tropopause temperature of ~ 1 K, with smaller, antiphased maxima centered near 30°S and 30°N and extending into the extratropics.

In contrast, NCEP 50–70 hPa zonal wind QBO zonal wind shear anomalies are of uniform sign for a given QBO wind regime across the range ~ 25°S–25°N, but are negligible outside of the tropics for this layer (Fig. 13). This is useful to keep in mind for interpreting seasonal synoptic charts of 70–150 hPa zonal wind shear in Section 4. The QBO range in 50–70 hPa wind shear is ~ 10 m s^{-1} per 20 hPa.

4. 2001: NCEP seasonal and geographical variation of QBO signal in the UTLS

4.1 NCEP tropopause temperature

The geographical distribution of seasonal mean and QBO W–E differences in NCEP tropopause temperature are shown for DJF and JJA in Fig. 14. Coldest temperatures during DJF occur over Amazonia, Central Africa, and the West Pacific warm pool, with temperatures less than 192 K over the Amazon and Western Pacific (Figs. 14e, f). These are the locations of chronic deep convection, characterized by low OLR and high rainfall rate (e.g., Collimore et al. 1998). During JJA, the Western Pacific deep convection shifts toward India, and Amazonian convection shifts toward the Gulf of Panama. Tropopause temperatures are 2–4 K warmer throughout the tropics during JJA, and there is less geographical variation compared to DJF (Figs. 14g, h). Slight variations in the pattern and magnitude of tropopause temperature are seen between 1958–1978 and 1979–2000 (compare Figs. 14e and f, g and h). These seasonal mean distributions agree well with those of Seidel et al. (2001, Fig. 11), who used radiosondes from 1961–1990, Highwood and Hoskins (1998, Fig. 6), who used ECMWF data from 1991–1995, and Hoinka (1999, Fig. 2), who used ECMWF data from 1979–1993.

Distributions of QBO W–E differences in tropopause temperature are shown for DJF and JJA in Figs. 14a–d. During QBO W, tropical tropopause temperatures are warmer, and subtropical temperatures are generally colder, in agreement with the zonal mean results shown in Figs. 10–13 and with theoretical expectations from the QBO MMC. Statistical significance is fairly high throughout the tropics, where the range reaches 1.5 K, and is somewhat smaller during JJA and during the second half of the data record. Another statistically significant zonal mean QBO signal is seen near 25°S during JJA, with the range reaching

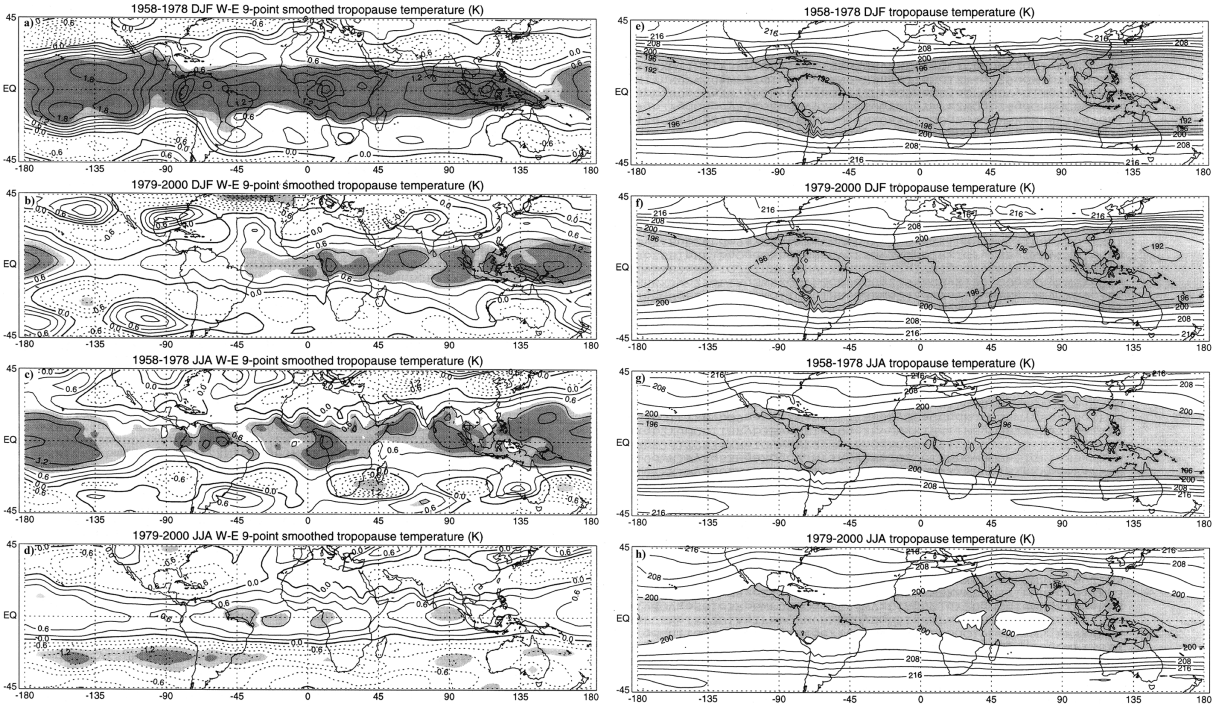

Fig. 14. Seasonally averaged (left, panels a–d): QBO W–E NCEP tropopause temperature (contour interval, 0.3 K; dashed contours, negative), and (right, panels e–h): NCEP mean tropopause temperature (contour interval, 3 K in the shaded regions below 200 K and 4 K elsewhere) for DJF (panels a, b, e, f) and for JJA (panels c, d, g, h). NCEP data during 1958–1978 and 1979–2000 are shown separately for each season (upper and lower of each pair). In the QBO W–E difference fields (left), light shading indicates confidence level above 90 %, dark shading above 95 %, and the fields have been smoothed once with a 9-point square filter.

1.5 K (Figs. 14c, d). In this case, the signal is larger during the second half of the data record. This pattern is reminiscent of the latitudinal antiphasing in the SH found by Angell and Korshover (1964) (Fig. 2).

Assuming that enhanced tropical upwelling is related to a cooler TTL, this zonal mean QBO signal is compatible with a reduction of the Brewer–Dobson circulation during QBO W. It is consistent with the results of Eluszkiewicz et al. (1996) and Yang and Tung (1996), who found that the global circulation in the lower stratosphere is weaker during QBO W, and with Seol and Yamazaki (1998), who showed that the upward mass flux across 100 hPa in the tropics is reduced during QBO W.

In addition to the zonal mean QBO signal, significant geographical variations, or zonal asymmetries, occur. These zonal asymmetries appear to be linked to the distribution of continents and seasonal monsoon structures. During DJF, the temperature range is largest in a band extending from South America, increasing eastward to ~ 1.6 K near Indonesia (Figs. 14a, b). The location of the maximum near Indonesia during DJF differs somewhat during the two periods (Figs. 14a, b). The maximum found in the eastern Pacific during 1958–1978 (Fig. 14a) is largely absent during 1979–2000 (Fig. 14b). During JJA (Figs. 14c, d), QBO W–E differences maximize over the Atlantic, Indian, and Pacific Oceans.

Zhou et al. (2001) interpolated global ECMWF data at standard pressure levels for the period 1979–1993 to estimate CPT levels. Daily values were then sorted by QBO phase according to a 40–70 hPa shear index, with a lag of 6 months. Their Fig. 7 shows the annual mean distributions of CPT temperatures for QBO W and QBO E in the latitude band 25°S–25°N. Differences of ~ 0.4–0.8 K occur, with a maximum in the Eastern Pacific.

Collimore et al. (2003) described QBO W–E differences for OLR and highly reflective cloud for each season, which showed reduced deep tropical clouds during QBO W. They also showed QBO W–E differences in tropopause temperature for each season using

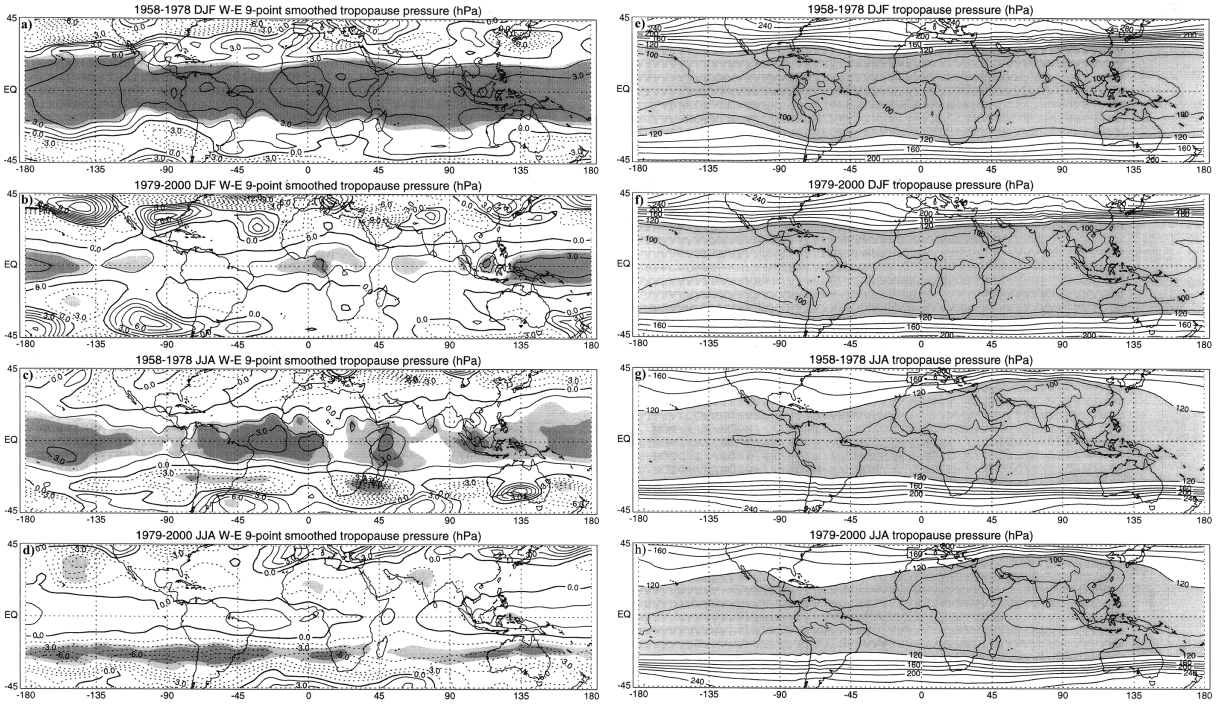

Fig. 15. As in Fig. 14, except for NCEP tropopause pressure. In the QBO W–E plots (left, panels a–d), the contour interval is 1.5 hPa, with dashed contours negative. Light shading indicates confidence level above 90 % and dark shading above 95 %. In QBO seasonal mean plots (right, panels e–h), the contour interval is 10 hPa in the shaded region below 120 hPa and 20 hPa elsewhere.

NCEP data from the 17-yr period of 971–1987 and using the 50–70 hPa shear index with no lag. They confined their presentation to the band 25°S–25°N, which excludes the antiphased subtropical features. Similar to the results of Zhou et al. (2001), their QBO range in the tropics showed a maximum in the Eastern Pacific. The sparseness of radiosonde observations in the Eastern Pacific renders a signal less reliable in this region. Perhaps over time better analysis methods and satellite temperature data have helped to ameliorate this problem. The seasonal and geographical dependence of the QBO signal in MERRA-2 CPT temperature and ERA-Interim data is explored in detail in Sections 5 and 6.

4.2 NCEP tropopause pressure

Climatological tropopause pressure and QBO W–E differences in tropopause pressure are shown for DJF and JJA in Fig. 15. Tropopause pressures are less than 100 hPa throughout most of the tropics during DJF (Figs. 15e, f) and near India during JJA (Figs. 15g, h). These seasonal mean tropopause pressure distributions agree well with Hoinka (1998, Fig. 2) and Seidel et al. (2001, Fig. 9).

Tropopause pressures are higher throughout the tropics during QBO W than during QBO E (Figs. 15a–d). This is compatible with the zonal mean results of Randel et al. (2000), shown in Fig. 11b, and with Fig. 3c of Collimore et al. (2003). As with tropopause temperature (Figs. 14a–d), differences in the tropics are larger and more statistically significant during DJF than in JJA, and during the first half of the data record. Again, significant zonal asymmetries are evident. QBO differences in tropopause pressure are larger over the Western Pacific during DJF (Figs. 15a, b) and over each of the three oceans during JJA (Figs. 15c, d). The QBO range in tropopause pressure exceeds ~ 3 hPa near Indonesia during DJF (Figs. 15a, b).

As with tropopause temperature, there is an interesting hemispheric asymmetry, with an amplified, statistically significant QBO signal in tropopause pressure near 25°S during JJA (Figs. 15c, d). This is especially notable during the second half of the data record, with a range exceeding ~ 6 hPa (Fig. 15d).

To relate changes in tropopause pressure to changes

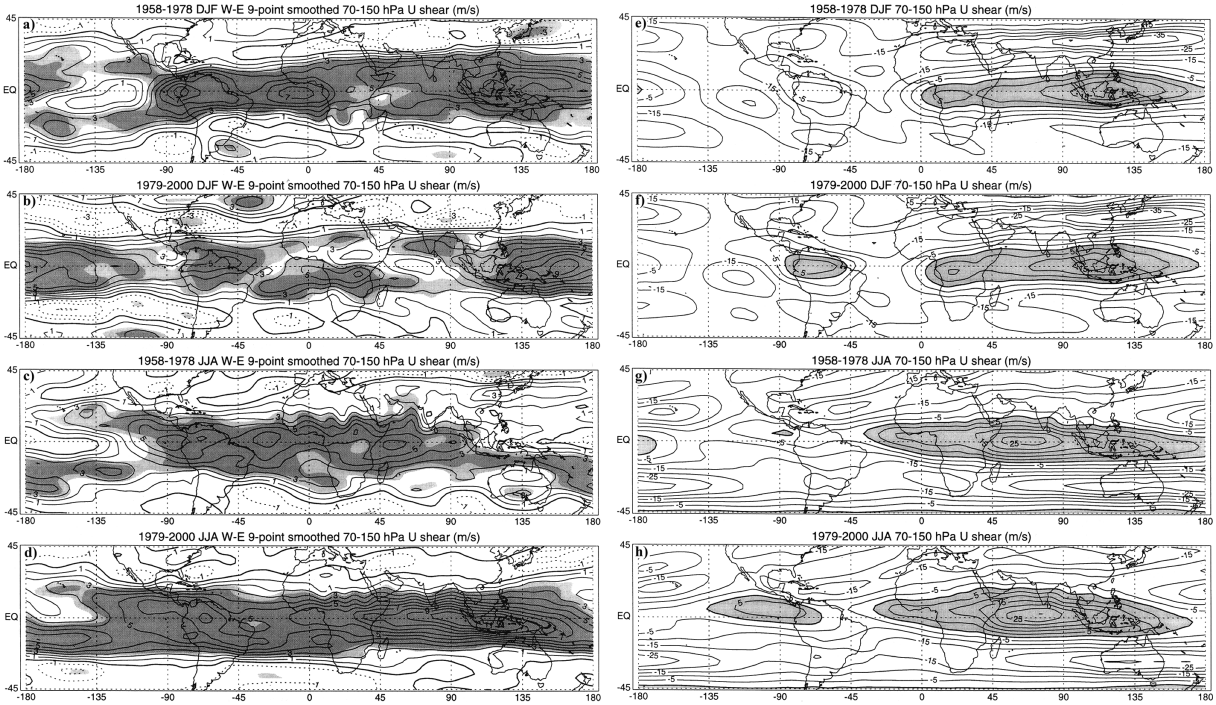

Fig. 16. As in Fig. 14, except of NCEP 70–150 hPa zonal wind shear. In the QBO W–E plots (left, panels a–d) the contour interval is 1 m s^{-1} (80 hPa)$^{-1}$, with dashed contours negative. Light shading indicates confidence level above 90 % and dark shading above 95 %. In seasonal mean plots (right, panels e–h), the contour interval is 5 m s^{-1} (80 hPa)$^{-1}$, with positive values shaded.

in tropopause altitude, one may use the hydrostatic equation $\delta p = -\rho g \delta z$. Assuming that $\rho \sim 0.1$ kg m^{-3} near the tropopause, an increase of 100 Pa (1 hPa) in tropopause pressure corresponds to a 100 m decrease in tropopause altitude. From Fig. 15, one might expect the tropical tropopause during QBO W to be ~ 100–300 m lower than average in DJF and ~ 100 m lower in JJA. This is compatible with the results of Reid and Gage (1985) shown in Fig. 4.

4.3 NCEP 70–150 hPa wind shear

The DJF and JJA average distributions of 70–150 hPa zonal wind shear are shown in Figs. 16e–h. This layer spans the depth of the TTL, as defined by Fueglistaler et al. (2009). Westerly shear is found over Amazonia and over a broad region extending from Africa to Indonesia, reaching 15 m s^{-1} per 80 hPa over Indonesia during DJF (Figs. 16e, f). This pattern is shifted slightly westward during JJA, reaching 25 m s^{-1} per 80 hPa over the Indian Ocean (Figs. 16g, h). During JJA, westerly shear is enhanced in the eastern hemisphere by the upper tropospheric easterlies that lie equatorward of the Tibetan High. Since seasonal mean winds are weak near 70 hPa, geographical and seasonal variations in 70–150 hPa shear are primarily due to variations at 150 hPa. The region of westerly shear over the Amazon is more robust in the second half of the data record (compare Fig. 14e with f, and g with h).

In the extratropics, 70–150 hPa wind shears are generally negative (Figs. 16e–h). The easterly shear and zonal variation in this pattern near ±30° is due to the presence of the SWJ, which varies in longitude and season. Strong easterly shear is found above the SWJ near 30°N during DJF, reaching −35 m s^{-1} per 80 hPa over Japan (Figs. 16e, f), and near 30°S over Australia during JJA (Figs. 16g, h).

QBO W–E differences in 70–150 hPa zonal wind shear for DJF and JJA are shown in Figs. 16a–d. The sign of the shear is retained so that one might visually add the QBO W–E perturbation to the seasonal average field and determine whether UTLS wind shear is diminished or enhanced locally by the QBO. During QBO W, 150–70 hPa wind shears are more westerly by 3–8 m s^{-1} per 80 hPa throughout most of the tropics (Figs. 16a–d), in agreement with the zonal

mean results in Fig. 13b. QBO differences in 70–150 hPa wind shear are generally statistically significant throughout the tropics. During DJF, maxima are found over Amazonia, Africa, and Indonesia (Figs. 16a, b), where the basic state shear is westerly (Figs. 16e, f). During JJA, a maximum is found extending from South America eastward to Indonesia (Figs. 16c, d). A notable difference is found between the two periods near New Guinea, where the QBO signal is larger during 1979–2000 (Figs. 16c, d).

The basic state 70–150 hPa wind shear over the subtropical North Atlantic during JJA is ~ −10 m s^{-1} to −15 m s^{-1} per 80 hPa (Figs. 16g, h). During QBO W, the predominant seasonal mean easterly shear in the subtropical North Atlantic would be diminished by ~ 1–3 m s^{-1} per 80 hPa (Figs. 16c, d, g, h). This type of information can be useful in considering Gray et al.'s (1992a) hypothesis that tropical deep convection, including tropical cyclones, might be more robust in reduced UTLS wind shear.

Considering the tropics, QBO E would act to diminish the westerly shear seen over centers of deep convection over Amazonia and from Africa to Indonesia (Figs. 16e–h). If Gray et al.'s hypothesis is correct, this would suggest that tropical deep convection would be enhanced in these regions during QBO E.

QBO W–E differences in 70–150 hPa shear exhibit a node near 25° latitude, with shears tending to be more easterly during QBO W near 30° latitude (Figs. 16a–d). Figure 13b shows that QBO differences in 50–70 hPa wind shear are negligible poleward of ~ 25° latitude. This suggests that the difference occurs at 150 hPa, with QBO W favoring stronger SWJs (which would make 70–150 hPa shears more easterly). The strength and seasonality of the observed QBO influence on the SWJs is reexamined using ERA-Interim data in Section 6.

The QBO signal in the tropical UTLS is less robust during 1978–2000 than during 1958–1978 in the NCEP record. This was previously shown in Figs. 13a and 14 of Randel et al. (2000). Recent comparisons of the zonal mean QBO signal in a range of global analyses also show that the NCEP signal during 1978–2000 is somewhat weaker than in other analyses (Tegtmeier et al. 2020; Martin et al. 2021).

The geographical variation of the QBO signal and its seasonal dependence as seen in NCEP data during 1958–1978 and 1979–2000 are now compared with two modern global reanalysis data sets. We first explore the seasonal QBO signal in tropopause temperature in MERRA-2 data for 1980–2017, focusing on the QBO range in CPT temperature in the deep tropics. This is followed by an analysis of results from ERA-Interim data in the domain 40°S–40°N, 1000-1 hPa, for the period 1979–2018.

5. QBO W–E MERRA-2 CPT temperature

Figure 17 shows the annual and seasonal mean distributions of the range in QBO W–E CPT temperatures in MERRA-2 analyses for the 38 years of 1980–2017, in the domain 20°S–20°N. In the annual mean (Fig. 17a), one may observe a broad equatorial maximum, with values reaching ~ 2 K near the west coast of South America, over Africa, and Indonesia. A node, or minimum in QBO range, is seen in MERRA-2 CPT temperature near ~ 15° latitude, where statistical significance can fall below 99 %. This is similar to the average latitude of the zero-line for QBO W–E tropopause temperature seen in Figs. 14a–d.

The QBO W–E range in MERRA-2 CPT temperature varies considerably with season, with larger values during DJF and MAM (Figs. 17b, c), contributing fundamentally to the geographical pattern seen in the annual average (Fig. 17a). During DJF, maxima are observed over the west coast of South America and stretching from Africa to Indonesia, with a secondary maximum over the Western Pacific (Fig. 17b). This zonally asymmetric pattern for DJF seen in MERRA-2 data is similar to what was found for the NCEP data (Figs. 14a, b), but with maximum amplitudes over Indonesia of ~ 2.2 K instead of ~ 1.8 K.

During MAM, the pattern is similar to that of DJF, but with a reduction in the Western Pacific and enhancement in the Eastern Pacific (compare Figs. 17b, c). Amplitudes during MAM are larger than during DJF near South America, and extending from Africa to Indonesia, reaching 2.5 K. It may be relevant that in March the coldest climatological temperatures occur over Africa (Tuck et al. 1993).

During JJA and SON, the QBO range in CPT is less than ~ 1.4 K. During JJA, a maximum occurs over the Atlantic/African sector, with a secondary maximum over Indonesia (Fig. 17d). This is in broad agreement with results from NCEP data (Figs. 14c, d). During SON, the pattern is similar to that of JJA in the Atlantic/African sector (Fig. 17e), but two other maxima occur over the west coast of South America and Western Pacific (Fig. 17e).

6. Analysis of ERA-Interim data during 1979–2018

6.1 ERA-Interim 100 hPa temperature

The geographical distributions of QBO W–E (phase-4 minus phase-8) differences for 100 hPa tem-

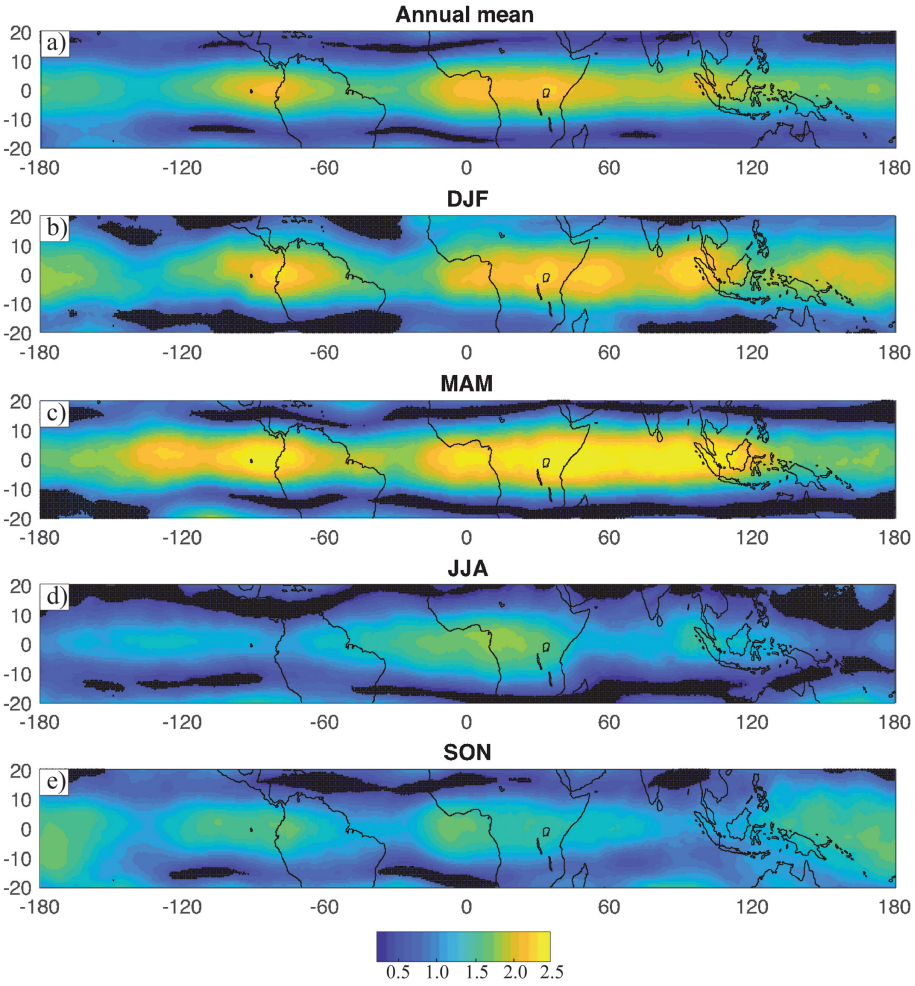

Fig. 17. QBO W–E range in MERRA-2 CPT temperature (color bar; contour interval, 0.125 K) for the 38-yr period of 1980–2017 for a) the annual mean, b) DJF, c) MAM, d) JJA, and e) SON. Regions with less than 99 % confidence are indicated in black.

perature in ERA-Interim data during 1979–2018 are shown for each season in Fig. 18. In agreement with results for NCEP and MERRA-2 tropopause temperatures, QBO differences in 100 hPa temperature have a significant zonal mean component, with a typical range of 1–2 K, and QBO W favoring higher 100 hPa temperatures in the tropics and lower temperatures in the subtropics.

Significant geographical variations are also evident. During DJF (Fig. 18a), QBO W–E differences are larger over Amazonia, Africa, and Indonesia, in a pattern similar to Figs. 14a, 14b and 17b. The range reaches 1.5 K over Indonesia during DJF in the ERA-Interim data (Fig. 18a).

During MAM (Fig. 18b), the statistically significant region in the tropics is much larger, extending from the far Eastern Pacific eastward to the Date Line, with largest ranges (1.5 K) over Amazonia, Africa, and Indonesia. Also of significance during MAM are the pronounced QBO W cold regions near 25°S and 25°N during QBO W, to be further discussed in Section 6.4.

During JJA (Fig. 18c), a QBO W–E range maximum extends from Brazil to East Africa, reaching 1.2 K, with a second maximum in the Eastern Indian Ocean. This is in agreement with Figs. 14c, 14d, and Fig. 17d. Note also the statistically significant negative region near 25°S during JJA (Fig. 18c), in agreement with results shown in Fig. 14d. During SON (Fig. 18d), tropical QBO differences are similar to in JJA, but with another maximum over the Eastern Pacific,

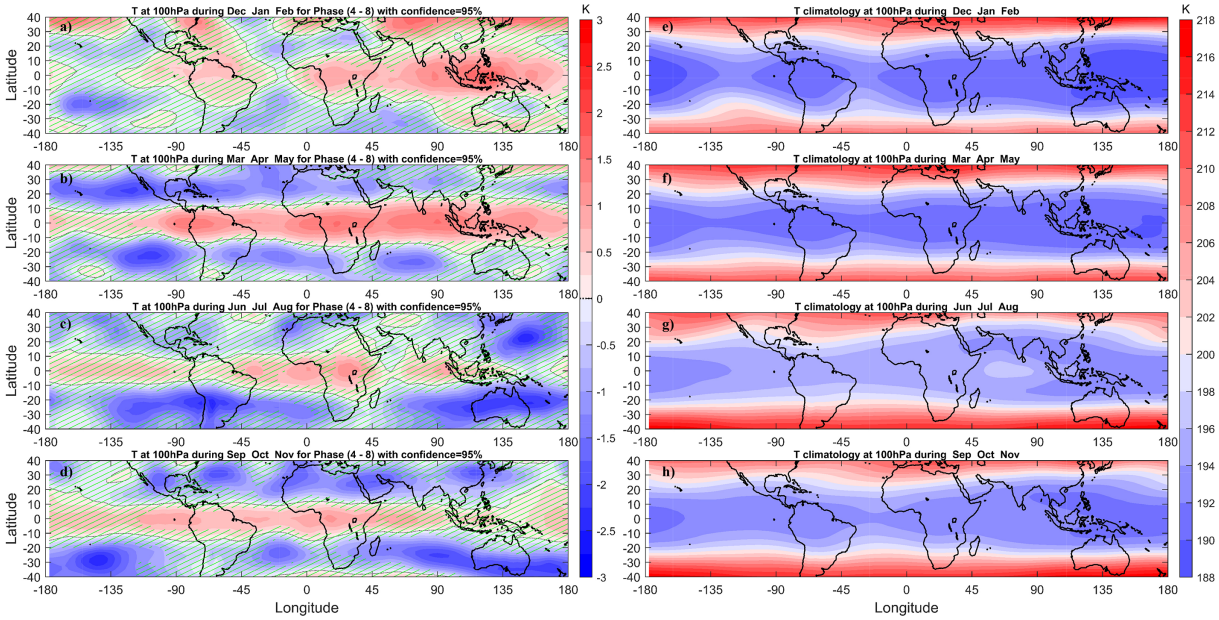

Fig. 18. Seasonal mean ERA-Interim 100 hPa temperature (left, panels a–d): QBO W–E differences (color bar; range −3 to 3 K; contour interval, 0.25 K) and (right, panels e–h): seasonal means (color bar; range 188 to 218 K; contour interval, 2 K), for DJF (a, e), MAM (b, f), JJA (c, g), and SON (d, h). Monthly mean data for the 40-yr period of 1979–2018 were analyzed using the EOF method of Wallace et al. (1993). QBO W–E values shown are phase-4 minus phase-8, which corresponds to W and E maxima in the lower stratosphere. Diagonal green lines indicate regions with less than 95 % statistical significance. In the left-hand panels, the zero line, or node, is indicated with a dotted black line.

in agreement with Fig. 17e. There is also evidence of a moderate QBO signal near 25°S and 25°N during SON (Fig. 18d), similar to that seen during MAM (Fig. 18c).

A detailed inspection of the QBO W–E signal in MERRA-2 CPT temperature (Fig. 17) and ERA-Interim 100 hPa temperature (Fig. 18), for each season, shows that they are remarkably similar in distribution and magnitude. These modern data sets confirm many of the features seen in the NCEP analysis, including a tendency for maxima to occur near centers of deep convection, and a large QBO range near 25°S during JJA. The antiphased response in the subtropics is most pronounced in the SH during JJA, and in both hemispheres during MAM and SON.

6.2 ERA-Interim 150 hPa zonal wind

The geographical distributions of seasonal means and QBO W–E differences in 150 hPa zonal wind are shown in Fig. 19. The 150 hPa level lies below the tropical tropopause, extends through the center of the SWJs near 30°S and 30°N, and into the extratropical lower stratosphere. During DJF, easterly flow is seen over Amazonia, Africa, and Indonesia, near regions of deep convection (Fig. 19e). Elsewhere, westerlies are observed, reaching maxima in the SWJs near 30°S and 30°N. During MAM, the pattern of easterlies is similar to that of DJF, but with reduced strength in the eastern hemisphere, and light westerlies over Amazonia (Fig. 19f). During JJA, the region of easterlies greatly expands and strengthens, extending from the Western Pacific westward to Brazil (Fig. 19g). This is consistent with the development of the Tibetan High during the northern hemisphere (NH) summer. Note also the center of easterlies over the far Eastern tropical Pacific, near the region of deep convection in the Gulf of Panama (Fig. 19g). During SON, the pattern is similar to JJA but somewhat reduced in amplitude and extent (Fig. 19h).

Seasonal mean patterns of NCEP 70–150 hPa zonal wind shear (for the period 1978–2000) and ERA-Interim 150 hPa zonal wind show good agreement between regions of westerly 70–150 shear and regions of 150 hPa easterlies for both DJF and JJA (compare Figs. 16e, f with 19e, and 16g, h with 19g). This lack of westerly shear over the far Eastern tropical Pacific

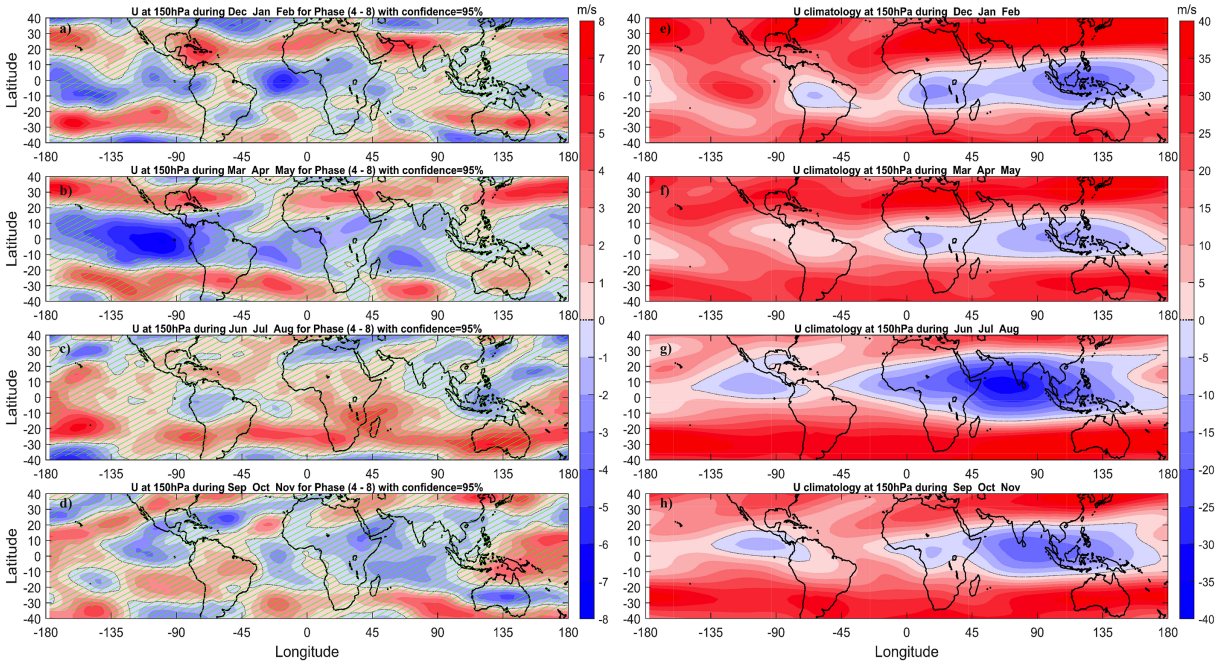

Fig. 19. As in Fig. 18, except of (left, panels a–d): QBO W–E differences in 150 hPa zonal wind (color bar; range −10 m s^{-1} to 10 m s^{-1}; contour interval, 1 m s^{-1}) and (right, panels e–g): seasonal mean distribution of 150 hPa zonal wind (color bar; range –40 m s^{-1} to 40 m s^{-1}; contour interval, 5 m s^{-1}). The zero contour is represented with a dotted black line.

in the 1958–1978 NCEP data (Figs. 16e, g) suggests that satellite data have since improved the accuracy of this feature.

During QBO W, the SWJs tend to be stronger in each season, with ranges of 1–7 m s^{-1}, but with variable statistical significance (Figs. 19a–d). During DJF (Fig. 19a), statistically significant differences are seen over the Caribbean, North Africa, and India in the NH, and over Australia and the mid-Pacific in the SH. Also of interest during DJF is the easterly anomaly over the tropical Atlantic for QBO W.

During MAM (Fig. 19b), the signal in both subtropics is more robust than during DJF, with centers of significant westerly enhancement of the SWJ over North Africa and from East Asia eastward to the Atlantic in the NH. Note the large easterly anomaly over the eastern tropical Pacific in the upper troposphere during QBO W in MAM (Fig. 19b). This is consistent with a reduced Walker circulation during QBO W, and tends to confirm Yasunari's (1989) suggestion that the QBO can modulate the Walker circulation.

During JJA (Fig 19c), the QBO signal in 150 hPa winds is generally weaker, except for a strong signal in the SH subtropics. During SON (Fig. 19d), the signal is similar to that of JJA, but weaker in the SH subtropics and stronger in the NH subtropics.

Wang et al. (2018), in an investigation of the QBO effect on NH storm tracks, showed meridional sections of zonal wind together with QBO W and QBO E anomalies, averaged for the Pacific and Atlantic sectors. They used ERA-Interim data averaged for October–March, during the period 1979–2016. Their Fig. 1 shows that QBO W strengthens the SWJ in both the Atlantic and Pacific sectors, but QBO E favors a poleward displacement in the Pacific sector. These results are consistent with Fig. 19a and with the numerical modeling results of Garfinkel and Hartmann (2007, 2011).

In summary, QBO W–E differences for ERA-Interim 150 hPa zonal winds tend to show an enhancement of the SWJs during QBO W. As with 100 hPa temperature, the response in the subtropics is most pronounced during MAM in both hemispheres and during JJA in the SH, with moderate signals during DJF in the NH and during SON in both hemispheres. More can be understood about this relationship by examining variation in the meridional plane throughout the UTLS.

6.3 *ERA-Interim seasonal structure of QBO anomalies in meridional plane*

Seasonal mean distributions of QBO W–E zonal mean anomalies of ERA-Interim zonal wind and temperature, with superimposed vectors of the MMC are shown in Fig. 20, for the domain 40°S–40°N, 1000–1 hPa. Each seasonal mean tropopause is also indicated. This depiction of phase-4 minus phase-8 selects for a positive westerly wind anomaly near 50 hPa (~ 21 km) over the equator, with an easterly maximum near 10 hPa (~ 30 km) and another westerly maximum near 2 hPa (~ 58 km), giving a vertical wavelength of ~ 27 km, as seen in each season (Figs. 20a–d).

The tropical westerly wind anomaly near 50 hPa exhibits an interesting poleward and downward extension into the subtropical UTLS near the SWJs. This effect is most noticeable in the SH during JJA (Fig. 20c) and during MAM in both hemispheres (Fig. 20b). More moderate effects are also seen in both hemispheres during DJF (Fig. 20a) and in the SH during SON (Fig. 20d). This signal in the zonal mean confirms QBO W–E features diagnosed in 150 hPa zonal wind (Fig. 19), and provides a broader context for the 150 hPa signal in terms of the QBO MMC.

During QBO W there is an extensive and statistically significant easterly zonal wind anomaly in the tropical upper troposphere, but only during DJF and MAM (Figs. 20a, b). During MAM, this negative anomaly reaches 3 m s^{-1} (Figs. 20b). This signal is a zonal average of the large negative anomaly in Figs. 19a, b, which reaches 9 m s^{-1} in the eastern tropical Pacific in MAM (Fig. 19b). The negative region spans the upper troposphere in the tropical eastern Pacific, the eastward half of the Walker circulation. During QBO W, the Walker circulation is reduced, especially during MAM. During MAM, there are also statistically significant warm temperature anomalies in the upper troposphere near 20°S and 20°N during QBO W (Fig. 20f), which are related to strengthening of the SWJ (Fig. 20d) through thermal wind balance. This has implications for the "East Pacific Tropical Rossby waveguide", where westerly winds associated with the Walker circulation allow Rossby wave energy to travel between hemispheres (Webster and Holton 1982). During MAM, this would be less likely to occur during QBO W.

QBO W–E equatorial positive temperature maxima occur near 70 hPa and 5 hPa, with a cold anomaly near 30 hPa (Figs. 20e–h). During the equinoxes (Figs. 20f, h), the temperature anomaly pattern is equatorially symmetric, in a 9-element "checkerboard" pattern centered on the tropical cold anomaly near 30 hPa, with stacked cells of the opposite sign maximizing near 30°S and 30°N and extending into midlatitudes.

During the solstices this pattern is warped, such that larger warm anomalies are found on the winter side near 30 hPa (Figs. 20e, g), which suggests that the QBO MMC is stronger in the winter subtropics. The MMC is also stronger on the winter side. This may be related to enhanced planetary wave drag in the subtropical winter hemisphere. This seasonal modulation of the QBO has been discussed by Randel et al. (1999), Kinnersley (1999), and Pena-Ortiz et al. (2008).

QBO W–E vertical motion anomalies are anticorrelated with the temperature anomalies due to adiabatic cooling/heating. This relationship is expected from a wave-driven circulation, where upward motion advects low potential temperature air upward, creating a cold anomaly. This "checkerboard" pattern of vertical motion comprises three stacked MMCs of alternating sign in the subtropics. These seasonal climatological meridional distributions provide an integrative view of QBO W–E anomalies of wind and temperature at different locations and latitudes, including the antiphased relationship between the tropical and subtropical UTLS.

6.4 *ERA-Interim time mean QBO anomalies of zonal wind, temperature, and MMC*

The time mean distribution of QBO W–E ERA-Interim zonal mean zonal wind, temperature, and MMC is shown in Fig. 21. The QBO range in zonal wind at the equator near 50 hPa is ~ 25 m s^{-1} (Fig. 21a). The QBO range in temperature at the equator near 70 hPa is ~ 2 K, with the warm anomaly extending below the tropopause (Fig. 21b). In the tropical upper troposphere, there is a statistically significant QBO signal with range exceeding 2 m s^{-1}, extending into the middle troposphere (Fig. 21b). This annual mean preserves some of the strong signal seen in MAM in Fig. 20b, which is largely due to a reduced eastward flow in the Eastern Pacific (Fig. 19c). Enhancement of the SWJs by ~ 2 m s^{-1} during QBO W is seen in Fig. 21a, with a statistically significant region extending downward into the troposphere. Statistical significance is higher for the QBO signal near the SWJs relative to Fig. 19 due to zonal and time averaging.

The time-mean QBO W–E temperature anomaly pattern (Fig. 21b) shows a "checkerboard" grid with a statistically significant warm anomaly during QBO W in the upper troposphere, consistent with reduced upwelling in the tropics. The time-mean QBO W–E vertical velocity anomaly pattern is the same as, but

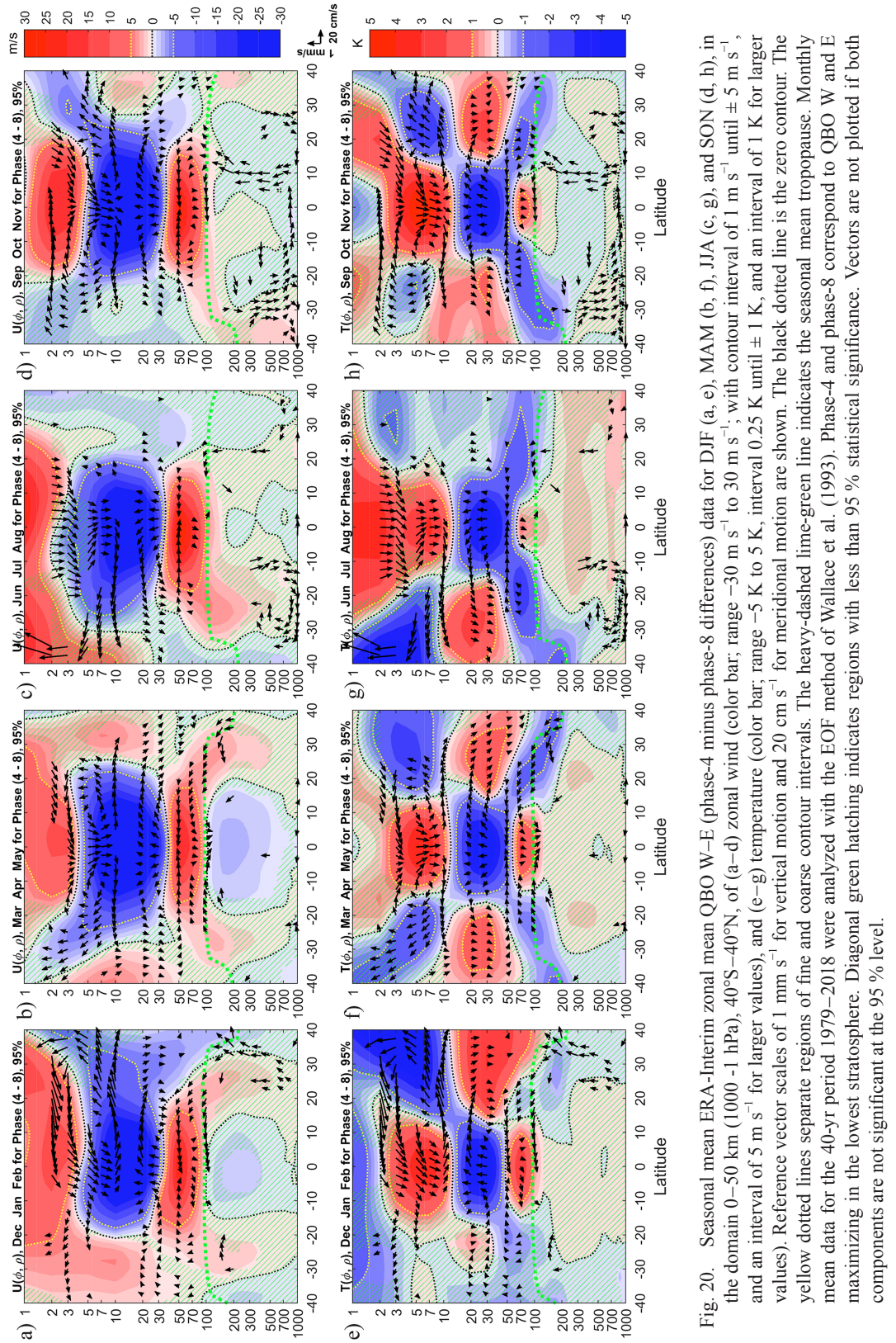

Fig. 20. Seasonal mean ERA-Interim zonal mean QBO W–E (phase-4 minus phase-8 differences) data for DJF (a, e), MAM (b, f), JJA (c, g), and SON (d, h), in the domain 0–50 km (1000 -1 hPa), 40°S–40°N, of (a–d) zonal wind (color bar; range −30 m s^{-1} to 30 m s^{-1}; with contour interval of 1 m s^{-1} until ± 5 m s^{-1}, and an interval of 5 m s^{-1} for larger values), and (e–g) temperature (color bar; range −5 K to 5 K, interval 0.25 K until ± 1 K, and an interval of 1 K for larger values). Reference vector scales of 1 mm s^{-1} for vertical motion and 20 cm s^{-1} for meridional motion are shown. The black dotted line is the zero contour. The yellow dotted lines separate regions of fine and coarse contour intervals. The heavy-dashed lime-green line indicates the seasonal mean tropopause. Monthly mean data for the 40-yr period 1979–2018 were analyzed with the EOF method of Wallace et al. (1993). Phase-4 and phase-8 correspond to QBO W and E maximizing in the lowest stratosphere. Diagonal green hatching indicates regions with less than 95 % statistical significance. Vectors are not plotted if both components are not significant at the 95 % level.

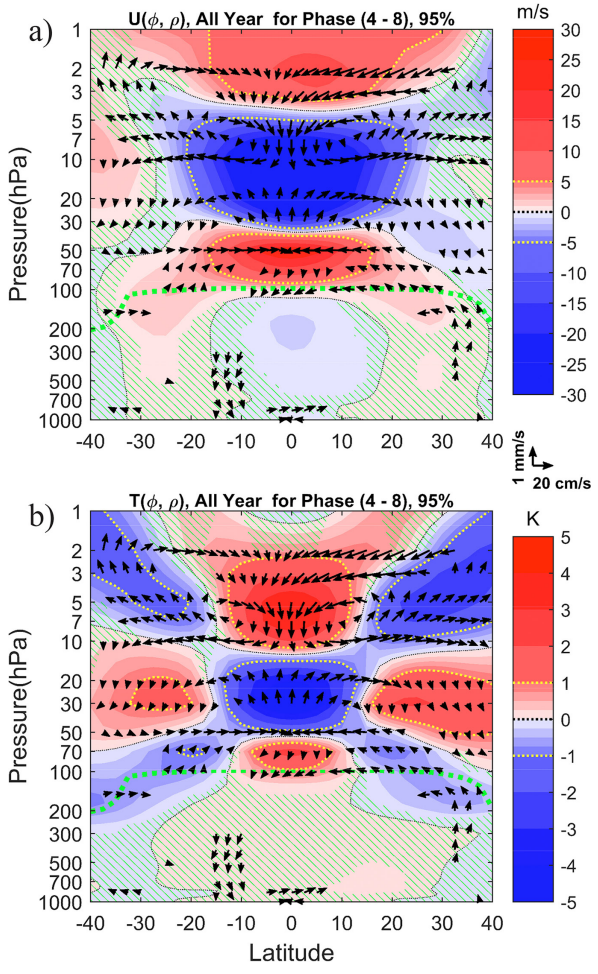

Fig. 21. Time mean ERA-Interim QBO W–E differences during the 40-yr period 1979–2018, in the domain 0–50 km (1000 -1 hPa), 40°S–40°N, for a) zonal wind (color bar; range −30 m s^{-1} to 30 m s^{-1}, with contour interval 1 m s^{-1} until ± 5 m s^{-1}, with interval 5 m s^{-1} for larger values), and b) temperature (color bar; range −5 K to 5 K, interval 0.25 K until ± 1 K, with interval 1 K for larger values). The reference vector scales of 1 mm s^{-1} for vertical motion and 20 cm s^{-1} for meridional motion are shown. The black dotted line is the zero contour. The yellow dotted lines separate regions of fine and coarse contour intervals. The heavy-dashed lime-green line indicates the time mean tropopause. Monthly mean data were analyzed with the EOF method of Wallace et al. (1993). Phases 4 and 8 correspond to QBO W and E maximizing in the lowest stratosphere. Diagonal green hatching indicates regions with less than 95 % statistical significance. Vectors are not plotted if both components are not significant at the 95 % level.

opposite in sign to, the temperature anomaly pattern (Fig. 21b). Note the statistically significant negative vertical velocity anomaly in the tropical upper troposphere and statistically significant positive anomalies near 100 hPa at 20°S and 20°N. This is compatible with a reduced Brewer–Dobson circulation in the lowest stratosphere during QBO W. A more complete description of this QBO temperature pattern is that a warm QBO anomaly in the TTL is accompanied by a cold anomaly that extends continuously poleward and downward all the way into the midlatitudes in the UTLS (note the downward-sloping cold maxima along the tropopause in Fig. 21b). By including all seasons, greater statistical significance is achieved, confirming the influence of the QBO on the SWJ, Hadley cell, and Walker circulation.

7. Summary of observational studies and discussion of mechanisms

7.1 Summary of observational results

Studies of radiosonde observations in the 1960s showed that the influence of the QBO extends downward into the tropical upper troposphere, modulating the altitude of the tropopause, and that antiphased temperature anomalies occur in the tropical and subtropical UTLS. Simultaneously, theoretical development showed that the QBO requires an MMC, the result of being wave-driven, and that this circulation spatially integrates features in altitude and latitude. The existence of a QBO MMC was confirmed in satellite-derived distributions of temperature and aerosol. Several authors suggested that the QBO might have other effects on tropical weather, including modulation of the Walker circulation, precipitation, and tropical cyclones. These studies raised the possibility that the QBO might somehow modulate tropical deep convection.

The advent of satellite data and global analyses allowed confirmation of the zonal mean QBO signal for tropopause temperature and pressure, with antiphased anomalies in the tropics and subtropics. During QBO W in the lower stratosphere, the tropical tropopause is lower and warmer, with stronger westerly wind shear in the tropics, stronger SWJs, and a weaker Walker circulation. During QBO E in the lower stratosphere, the tropical tropopause is higher and colder, with enhanced easterly wind shear in the tropics and a stronger Walker circulation. Seasonal maps of NCEP QBO W–E differences in tropopause temperature and pressure showed that the subtropical anomaly is largest in the winter hemisphere. They also showed that the QBO range in tropopause temperature exhibits

significant geographical variation, with largest values over centers of deep tropical convection, most notably over Amazonia, Africa, and Indonesia during DJF and over the Atlantic and Indian Oceans during JJA. These results suggest that there is some form of coupling between the QBO and tropical deep convection.

A modern update and extension of this analysis was shown using 38 years of MERRA-2 CPT data in the deep tropics, and 40 years of ERA-Interim data from 1979–2018, where months with a significant ENSO signal were removed from the record. Keeping in mind that the tropopause is not the same as the 100 hPa surface, that the QBO sorting algorithms were slightly different, and that the time periods were different, the salient features from the NCEP study were confirmed, including seasonal and geographical variation of the QBO temperature response and a strong signal in the SH winter subtropics. Improved statistical significance and data reliability provides greater confidence in interpreting results, with QBO W–E range in temperature anomalies of ~ 1–2.5 K. The detailed agreement in shape and magnitude for the MERRA-2 and ERA-Interim results for QBO W–E temperatures for each season supports the likelihood that these QBO signals are real.

Further information was gained from the modern data sets regarding the equinoctial seasons and modification of the SWJs. New results include 1) the existence of statistically significant QBO zonal wind and temperature anomalies in the upper troposphere, 2) a more complete, quantitative representation of the relationship among QBO temperature, zonal wind, and the MMC as a function of Season, 3) a time mean QBO structure diagram quantified by latitude, altitude, and amplitude, 4) evidence that the subtropical signal is largest during JJA in the SH, is large during MAM in both hemispheres, and is moderate in the NH during DJF, 5) evidence that the eastward flow in the upper troposphere over the Pacific Ocean (Walker circulation) is reduced by ~ 5–10 m s^{-1} during QBO W in MAM.

Accumulation of observational knowledge about QBO effects on the tropical and subtropical UTLS over the past 60 years has led to a more complete and quantified picture. Independent results for QBO W–E tropopause temperature confirm findings that the QBO signal tends to be larger in areas of tropical deep convection. Since observational analyses persistently indicate the existence of a "direct effect" of the QBO on the UTLS, it is worthwhile to consider possible physical mechanisms that could explain the coupling.

7.2 Mechanisms for a "direct effect" of the QBO

The observations reviewed here suggest that a primary physical process involved is simply that the zonal mean temperature anomalies are fundamentally associated with the wave-driven QBO MMC, including antiphasing between the tropics and subtropics, and the existence of QBO anomalies extending into the upper troposphere. This seems to be the primary physical cause of zonal mean QBO anomalies in the UTLS. Yet the enhanced QBO signal near areas of chronic deep convection and the influence on the Walker circulation argue in favor of an effect on deep convection. Collimore et al. (2003) reported that deep convection, as indicated by OLR and highly reflective cloud, is enhanced over Amazonia, Africa, and Indonesia during QBO E and diminished during QBO W. Other authors report a diminution of rainfall over Indonesia during QBO W (Liess and Geller 2012).

Three hypotheses have emerged in the literature that suggest physical mechanisms linking the QBO to deep convection, which are related to TTL temperature and thermodynamic efficiency, UTLS vertical wind shear, and UTLS inertial stability.

1) TTL temperature Emanuel (1986) suggested that the thermodynamic efficiency of organized deep convection may be enhanced if the tropopause is higher and colder. Gray et al. (1992b), Giorgetta et al. (1999), and others have suggested that the QBO modulates the static stability environment of deep convection in the UTLS, leading to the promotion or inhibition of convective strength and vertical penetration. If a cold QBO anomaly lies in the TTL, convective complexes may grow more efficiently, penetrating to greater altitudes, locally amplifying the zonal mean QBO cold anomaly.

2) UTLS wind shear The influence of QBO-induced differences in vertical wind shear in the UTLS on the development of deep convection and tropical cyclones has been explored by Gray (1968), McBride and Zehr (1981), Gray and Scheaffer (1991), Gray et al. (1992a, b), DeMaria and Kaplan (1994), and DeMaria (1996), and Frank and Ritchie (1999). They argue that increased wind shear in the UTLS tends to dynamically disrupt deep convection.

3) UTLS inertial stability Merrill (1988) suggested that the strength of a tropical cyclone can be enhanced by weak inertial stability (reduced lateral resistance) in the UTLS outflow layer. Montgomery and Farrell (1993) and Mecikalski and Tripoli (1998) found that mass divergence is facilitated in quadrants of tropical cyclones where inertial stability is reduced.

Giorgetta et al. (1999) imposed QBO wind shear

regimes in the UTLS in a general circulation model and found that QBO E favors more cloudiness over Indonesia. Their stated hypothesis is that the MMC associated with the imposed QBO anomalies created UTLS temperature anomalies, which modified the static stability environment (Grise et al. 2010) and were amplified by deep cloud feedback, supporting hypothesis 1).

In considering the observed signal, with regard to an amplified QBO effect over areas of tropical deep convection, maxima in QBO W–E tropopause temperature amplitude tends to coincide with areas of deep convection. However, the climatological centers of 70–150 hPa westerly shear (Fig. 16) and climatological centers of 150 hPa easterly winds (Fig. 19) also tend to coincide with regions of chronic deep convection. The fact that the TTL exhibits time mean easterlies over Amazonia, Africa, and Indonesia may be related to the existence of deep convection, which can transport easterly momentum from the trade winds to the UTLS. This structure is also compatible with the steady-state "Gill solution" for planetary wave structure in the tropical UTLS associated with a center of tropical heating (Gill 1980), where westward flow is expected over and to the west of an area of deep convection (see their Fig. 1 for equatorially centered convection and Fig. 3 for off-equatorial convection, similar to over Southeast Asia during JJA). An imposed QBO W shear anomaly would increase the shear in the UTLS over convective centers under hypothesis 2), tending to "disrupt" the vigor of convection, while QBO E would decrease the shear in the UTLS, promoting the robustness of convection.

The geographical distribution of the QBO signal in tropical TTL temperature is compatible with an amplification during QBO E when the TTL is cold and UTLS shear is reduced, and diminution during QBO W when the TTL is warm and UTLS shear is enhanced. This tropical regime should be contrasted with the subtropical UTLS environment of tropical cyclones, where typical easterly shears prevail (Figs. 16e–h, 19e–h), and QBO W can, in some regions and seasons, diminish UTLS shear and enhance it in others.

This simple geographical comparison supports the idea that tropical deep convection may act as a positive feedback mechanism on a QBO zonal mean temperature anomaly, in concert with changes in TTL wind shear, through an increase (QBO E) or decrease (QBO W) in the efficiency of tropical deep convection. Due to the importance of the tropics to global weather and climate, it is of interest to study the QBO "direct effect" in more detail from modeling, theoretical, and observational points of view to better understand the cause of these phenomena.

Acknowledgments

We would like to thank Stefan Hastenrath for providing tables of Berson's data, Amihan Huesmann for creating Figs. 14–16, Shellie Rowe for help with refining the figures, and the Editor and two anonymous reviewers for helpful suggestions. MHH acknowledges support from NSF grants AGS-1555851 and AGS-1947658. This review is a contribution to the SATIO-TCS (Stratospheric and Tropospheric Influences on Tropical Convective Systems) initiative in SPARC (Stratosphere–troposphere Processes and their Role in Climate).

References

Andrews, D. G., J. R. Holton, and C. B. Leovy, 1987: *Middle Atmosphere Dynamics*. Academic Press, San Diego, Calif., 489 pp.

Angell, J. K., and J. Korshover, 1964: Quasi-biennial variations in temperature, total ozone, and tropopause height. *J. Atmos. Sci.*, **21**, 479–492.

Angell, J. K., and J. Korshover, 1970: Quasi-biennial, annual, and semiannual zonal wind and temperature harmonic amplitudes and phases in the stratosphere and low mesosphere of the Northern Hemisphere. *J. Geophys. Res.*, **75**, 543–550.

Angell, J. K., and J. Korshover, 1974: Quasi-biennial and long-term fluctuations in tropopause pressure and temperature, and the relation to stratospheric water vapor content. *Mon. Wea. Rev.*, **102**, 29–34.

Angell, J. K., J. Korshover, and G. F. Cotten, 1969: Quasi-biennial variations in the "centers of action". *Mon. Wea. Rev.*, **97**, 867–872.

Anstey, J. A., and T. G. Shepherd, 2014: High-latitude influence of the quasi-biennial oscillation. *Quart. J. Roy. Meteor. Soc.*, **140**, 1–21.

Attard, H. E., and L. Coy, 2019: Connections between the stratosphere and synoptic variability. *US CLIVAR Variations*, **17**, 1–6.

Baldwin, M. P., and T. J. Dunkerton, 1999: Propagation of the Arctic Oscillation from the stratosphere to the troposphere. *J. Geophys. Res.*, **104**, 30937–30946.

Baldwin, M. P., L. J. Gray, T. J. Dunkerton, K. Hamilton, P. H. Haynes, W. J. Randel, J. R. Holton, M. J. Alexander, I. Hirota, T. Horinouchi, D. B. A. Jones, J. S. Kinnersley, C. Marquardt, K. Sato, and M. Takahashi, 2001: The quasi-biennial oscillation. *Rev. Geophys.*, **39**, 179–229.

Berrisford, P., P. Kållberg, S. Kobayashi, D. Dee, S. Uppala, A. J. Simmons, P. Poli, and H. Sato, 2011: Atmospheric conservation properties in ERA-Interim. *Quart. J.*

Roy. Meteor. Soc., **137**, 1381–1399.

Berson, A., 1910: *Bericht über die aerologische expedition nach Ostfrika im Jahre 1908.* Erstattet von ihrem Leiter Arthur Berson, Braunschweig, 119 pp.

Boville, B. A., 1984: The influence of the polar night jet on the tropospheric circulation in a GCM. *J. Atmos. Sci.*, **41**, 1132–1142.

Brönniman, S., and A. Stickler, 2013: Aerological observations in the tropics in the early twentieth century. *Meteor Z.*, **22**, 349–358.

Camargo, S. J., and A. H. Sobel, 2010: Revisiting the influence of the quasi-biennial oscillation on tropical cyclone activity. *J. Climate*, **23**, 5810–5825.

Choi, W., H. Lee, W. B. Grant, J. H. Park, J. R. Holton, K.-M. Lee, and B. Naujokat, 2002: On the secondary meridional circulation associated with the quasi-biennial oscillation. *Tellus B*, **54**, 395–406.

Collimore, C. C., M. H. Hitchman, and D. W. Martin, 1998: Is there a quasi-biennial oscillation in tropical deep convection? *Geophys. Res. Lett.*, **25**, 333–336.

Collimore, C. C., D. W. Martin, M. H. Hitchman, A. Huesmann, and D. E. Waliser, 2003: On the relationship between the QBO and tropical deep convection. *J. Climate*, **16**, 2552–2568.

Coy, L., P. A. Newman, S. Pawson, and L. R. Lait, 2017: Dynamics of the disrupted 2015/16 quasi-biennial oscillation. *J. Climate*, **30**, 5661–5674.

Dee, D. P., S. M. Uppala, A. J. Simmons, P. Berrisford, P. Poli, S. Kobayashi, U. Andrae, M. A. Balmaseda, G. Balsamo, P. Bauer, P. Bechtold, A. C. M. Beljaars, L. van de Berg, J. Bidlot, N. Bormann, C. Delsol, R. Dragani, M. Fuentes, A. J. Geer, L. Haimberger, S. B. Healy, H. Hersbach, E. V. Hólm, L. Isaksen, P. Kållberg, M. Köhler, M. Matricardi, A. P. McNally, B. M. Monge-Sanz, J.-J. Morcrette, B.-K. Park, C. Peubey, P. de Rosnay, C. Tavolato, J.-N. Thépaut, and F. Vitart, 2011: The ERA-Interim reanalysis: configuration and performance of the data assimilation system. *Quart. J. Roy. Meteor. Soc.*, **137**, 553–597.

DeMaria, M., 1996: The effect of vertical shear on tropical cyclone intensity change. *J. Atmos. Sci.*, **53**, 2076–2088.

DeMaria, M., and J. Kaplan, 1994: A statistical hurricane intensity prediction scheme (SHIPS) for the Atlantic basin. *Wea. Forecasting*, **9**, 209–220.

Dessler, A. E., S. P. Palm, and J. D. Spinhirne, 2006: Tropical cloud-top height distributions revealed by the Ice, Cloud, and Land Elevation Satellite (ICESat)/Geoscience Laser Altimeter Systerm (GLAS). *J. Geophys. Res.*, **111**, D12215, doi:10.10129/2005JD006705.

Dickinson, R. E., 1968: On the excitation and propagation of zonal winds in an atmosphere with Newtonian cooling. *J. Atmos. Sci.*, **25**, 269–279.

Dunkerton, T. J., 1983: Laterally-propagating Rossby waves in the easterly acceleration phase of the quasi-biennial oscillation. *Atmos.-Ocean*, **21**, 55–68.

Dunkerton, T. J., 2017: Nearly identical cycles of the quasi-biennial oscillation in the equatorial lower stratosphere. *J. Geophys. Res.: Atmos.*, **122**, 8467–8493.

Eluszkiewicz, J., D. Crisp, R. Zurek, L. Elson, E. Fishbein, L. Froldevaux, J. Waters, R. G. Grainger, A. Lambert, R. Harwood, and G. Peckham, 1996: Residual circulation in the stratosphere and lower mesosphere as diagnosed from Microwave Limb Sounder data. *J. Atmos. Sci.*, **53**, 217–240.

Emanuel, K. A., 1986: An air-sea interaction theory for tropical cyclones. Part I: Steady-state maintenance. *J. Atmos. Sci.*, **43**, 585–605.

Folkins, I., M. Loewenstein, J. Podolske, S. J. Oltmans, and M. Proffitt, 1999: A barrier to vertical mixing at 14 km in the tropics: Evidence from ozonesondes and aircraft measurements. *J. Geophys. Res.*, **104**, 22095–22102.

Fraedrich, K., S. Pawson, and R. Wang, 1993: An EOF analysis of the vertical-time delay structure of the quasi-biennial oscillation. *J. Atmos. Sci.*, **50**, 3357–3365.

Frank, W. M., and E. A. Ritchie, 1999: Effects of environmental flow upon tropical cyclone structure. *Mon. Wea. Rev.*, **127**, 2044–2061.

Fueglistaler, S., A. E. Dessler, T. J. Dunkerton, I. Folkins, Q. Fu, and P. W. Mote, 2009: Tropical tropopause layer. *Rev. Geophys.*, **47**, RG1004, doi:10.1029/2008RG000267.

Garfinkel, C. I., and D. L. Hartmann, 2007: Effects of the El Niño–Southern Oscillation and the Quasi-Biennial Oscillation on polar temperatures in the stratosphere. *J. Geophys. Res.*, **112**, D19112, doi:10.1029/2007JD008481.

Garfinkel, C. I., and D. L. Hartmann, 2011: The influence of the quasi-biennial oscillation on the troposphere in winter in a hierarchy of models. Part I: Simplified dry GCMs. *J. Atmos. Sci.*, **68**, 1273–1289.

Gettelman, A., and P. M. de F. Forster, 2002: A climatology of the tropical tropopause layer. *J. Meteor. Soc. Japan*, **80**, 911–924.

Gettelman, A., M. L. Salby, and F. Sassi, 2002: Distribution and influence of convection in the tropical tropopause region. *J. Geophys. Res.*, **107**, ACL 6-1–ACL 6-12.

Gill, A. E., 1980: Some simple solutions for heat-induced tropical circulation. *Quart. J. Roy. Meteor. Soc.*, **106**, 447–462.

Gille, J. C., and J. M. Russell III, 1984: The Limb Infrared Monitor of the Stratosphere: Experiment description, performance, and results. *J. Geophys. Res.*, **89**, 5125–5140.

Giorgetta, M. A., L. Bengtsson, and K. Arpe, 1999: An investigation of QBO signals in the east Asian and Indian monsoon in GCM experiments. *Climate Dyn.*, **15**, 435–450.

Gray, L. J., J. A. Anstey, Y. Kawatani, H. Lu, S. Osprey, and V. Schenzinger, 2018: Surface impacts of the Quasi Biennial Oscillation. *Atmos. Chem. Phys.*, **18**, 8227–

8247.

Gray, W. M., 1968: Global view of the origin of tropical disturbances and storms. *Mon. Wea. Rev.*, **96**, 669–700.

Gray, W. M., 1984: Atlantic seasonal hurricane frequency. Part I: El Niño and 30 mb Quasi-Biennial Oscillation influences. *Mon. Wea. Rev.*, **112**, 1649–1668.

Gray, W. M, and J. D. Sheaffer, 1991: El Niño and QBO influences on tropical cyclone activity. *Teleconnections Linking Worldwide Climate Anomalies*. Glantz, M., R. W. Katz, and N. Nicholls (eds.), Cambridge University Press, 257–284.

Gray, W. M., C. W. Landsea, P. W. Mielke, Jr., and K. J. Berry, 1992a: Predicting Atlantic seasonal hurricane activity 6-11 months in advance. *Wea. Forecasting*, **7**, 440–455.

Gray, W. M., J. D. Scheaffer, and J. A. Knaff, 1992b: Influence of the stratospheric QBO on ENSO variability. *J. Meteor. Soc. Japan*, **70**, 975–995.

Grise, K. M., D. W. J. Thompson, and T. Birner, 2010: A global survey of static stability in the stratosphere and upper troposphere. *J. Climate*, **23**, 2275–2292.

Hamilton, K., 2012: Sereno Bishop, Rollo Russell, Bishop's Ring and the discovery of the "Krakatoa easterlies". *Atmos.-Ocean*, **50**, 169–175.

Hastenrath, S., 1990: The relationship of highly reflective clouds to tropical climate anomalies. *J. Climate*, **3**, 353–365.

Hastenrath, S., 2007: Equatorial zonal circulations: Historical perspectives. *Dyn. Atmos. Oceans*, **43**, 16–24.

Haynes, P. H., P. Hitchcock, M. H. Hitchman, S. Yoden, H. Hendon, G. Kiladis, K. Kodera, and I. Simpson, 2021: The influence of the stratosphere on the tropical troposphere. *J. Meteor. Soc. Japan*, **99**, printing, doi: 10.2151/jmsj.2021-040.

Highwood, E. J., and B. J. Hoskins, 1998: The tropical tropopause. *Quart. J. Roy. Meteor. Soc.*, **124**, 1579–1604.

Hitchman, M. H., and C. B. Leovy, 1986: Evolution of the zonal mean state in the equatorial middle atmosphere during October 1978–May 1979. *J. Atmos. Sci.*, **43**, 3159–3176.

Hitchman, M. H., M. McKay, and C. R. Trepte, 1994: A climatology of stratospheric aerosol. *J. Geophys. Res.*, **99**, 20689–20700.

Ho, C.-H., H.-S. Kim, J.-H. Jeong, and S.-W. Son, 2009: Influence of stratospheric quasi-biennial oscillation on tropical cyclone tracks in the western North Pacific. *Geophys. Res. Lett.*, **36**, L06702, doi:10.1029/2009GL037163.

Hoerling, M. P., T. D. Schaack, and A. J. Lenzen, 1991: Global objective tropopause analysis. *Mon. Wea. Rev.*, **119**, 1816–1831.

Hoinka, K. P., 1998: Statistics of the global tropopause pressure. *Mon. Wea. Rev.*, **126**, 3303–3325.

Hoinka, K. P., 1999: Temperature, humidity, and wind at the global tropopause. *Mon. Wea. Rev.*, **127**, 2248–2265.

Holton, J. R., and H.-C. Tan, 1980: The influence of the equatorial quasi-biennial oscillation on the global circulation at 50 mb. *J. Atmos. Sci.*, **37**, 2200–2208.

Huesmann, A., and M. H. Hitchman, 2001: The stratospheric quasi-biennial oscillation in the NCEP reanalyses: Climatological structures. *J. Geophys. Res.*, **106**, 11859–11874.

Huesmann, A. S., and M. H. Hitchman, 2003: The 1978 shift in the NCEP reanalysis stratospheric quasi-biennial oscillation. *Geophys, Res. Lett.*, **30**, 1048, doi:10.1029/2002GL016323.

Kalnay, E., M. Kanamitsu, R. Kistler, W. Collins, D. Deaven, L. Gandin, M. Iredell, S. Saha, G. White, J. Woollen, Y. Zhu, M. Chelliah, W. Ebisuzaki, W. Higgins, J. Janowiak, K. C. Mo, C. Ropelewski, J. Wang, A. Leetmaa, R. Reynolds, R. Jenne, and D. Joseph, 1996: The NCEP /NCAR 40-year reanalysis project. *Bull. Amer. Meter. Soc.*, **77**, 437–472.

Kane, R. P., 1995: Quasi-biennial and quasi-triennial oscillations in the summer monsoon rainfall of the meteorological subdivisions of India. *Mon. Wea. Rev.*, **123**, 1178–1184.

Kawatani, Y., K. Hamilton, K. Miyazaki, M. Fujiwara, and J. A. Anstey, 2016: Representation of the tropical stratospheric zonal wind in global atmospheric reanalyses. *Atmos. Chem. Phys.*, **16**, 6681–6699.

Kinnersley, J. S., 1999: Seasonal asymmetry of the low- and middle-latitude QBO circulation anomaly. *J. Atmos. Sci.*, **56**, 1140–1153.

Kistler, R., E. Kalnay, W. Collins, S. Saha, G. White, J. Woollen, M. Chelliah, W. Ebisuzaki, M. Kanamitsu, V. Kousky, H. van den Dool, R. Jenne, and M. Fiorino, 2001: The NCEP-NCAR 50-year reanalysis: Monthly means CD-ROM and documentation. *Bull. Amer. Meteor. Soc.*, **82**, 247–268.

Knaff, J. A., 1993: Evidence of a stratospheric QBO modulation of tropical convection. *Atmos. Sci. Pap.*, **520**, 95 pp.

Liess, S., and M. A. Geller, 2012: On the relationship between QBO and distribution of tropical deep convection. *J. Geophys. Res.*, **117**, D03108, doi:10.1029/2011JD016317.

Lindzen, R. S., and J. R. Holton, 1968: A theory of the quasi-biennial oscillation. *J. Atmos. Sci.*, **25**, 1095–1107.

Lu, H., M. H. Hitchman, L. J. Gray, J. A. Anstey, and S. M. Osprey, 2020: On the role of Rossby wave breaking in the quasi-biennial modulation of the stratospheric polar vortex during boreal winter. *Quart. J. Roy. Meteor. Soc.*, **146**, 1939–1959.

Martin, Z., A. Sobel, A. Butler, and S. Wang, 2021: Variability in QBO temperature anomalies on annual and decadal time scales. *J. Climate*, **34**, 589–605.

Match, A., and S. Fueglistaler, 2019: The buffer zone of the quasi-biennial oscillation. *J. Atmos. Sci.*, **76**, 3553–3567.

McBride, J. L., and R. Zehr, 1981: Observational analysis of tropical cyclone formation. Part II: Comparison of

non-developing versus developing systems. *J. Atmos. Sci.*, **38**, 1132–1151.

McCormick, M. P., J. M. Zawodny, R. E. Veiga, J. C. Larsen, and P. H. Wang, 1989: An overview of SAGE I and SAGE II ozone measurements. *Planet. Space Sci.*, **37**, 1567–1586.

Mecikalski, J. R., and G. J. Tripoli, 1998: Inertial available kinetic energy and the dynamics of tropical plume formation. *Mon. Wea. Rev.*, **126**, 2200–2216.

Merrill, R. T., 1988: Environmental influences on hurricane intensification. *J. Atmos. Sci.*, **45**, 1678–1687.

Montgomery, M. T., and B. F. Farrell, 1993: Tropical cyclone formation. *J. Atmos. Sci.*, **50**, 285–310.

Newell, R. E., J. W. Kidson, D. G. Vincent, and G. J. Boer, 1974: *The General Circulation of the Tropical Atmosphere and Interactions with Extratropical Latitudes. Vol. 2*. MIT Press, Cambridge, USA, 371 pp.

Newman, P. A., L. Coy, S. Pawson, and L. R. Lait, 2016: The anomalous change in the QBO in 2015–2016. *Geophys. Res. Lett.*, **43**, 8791–8797.

Osprey, S. M., N. Butchart, J. R. Knight, A. A. Scaife, K. Hamilton, J. A. Anstey, V. Schenzinger, and C. Zhang, 2016: An unexpected disruption of the atmospheric quasi-biennial oscillation. *Science*, **353**, 1424–1427.

Pawson, S., and M. Fiorino, 1999: A comparison of reanalyses in the tropical stratosphere. Part 3: Inclusion of the pre-satellite data era. *Climate Dyn.*, **15**, 241–250.

Peña-Ortiz, C., P. Ribera, R. Garcia-Herrera, M. A. Giorgetta, and R. R. García, 2008: Forcing mechanism of the seasonally asymmetric quasi-biennial oscillation secondary circulation in ERA-40 and MAECHAM5. *J. Geophys. Res.*, **113**, D16103, doi:10.1029/2007JD009288.

Plumb, R. A., and R. C. Bell, 1982: A model of the quasi-biennial oscillation on an equatorial beta-plane. *Quart. J. Roy. Meteor. Soc.*, **108**, 335–352.

Randel, W. J., F. Wu, R. Swinbank, J. Nash, and A. O'Neill, 1999: Global QBO circulation derived from UKMO stratospheric analyses. *J. Atmos. Sci.*, **56**, 457–474.

Randel, W. J., F. Wu, and D. J. Gaffen, 2000: Interannual variability of the tropical tropopause derived from radiosonde data and NCEP reanalyses. *J. Geophys. Res.*, **105**, 15509–15523.

Reid, G. C., 1994: Seasonal and interannual temperature variations in the tropical stratosphere. *J. Geophys. Res.*, **99**, 18923–18932.

Reid, G. C., and K. S. Gage, 1985: Interannual variations in the height of the tropical tropopause. *J. Geophys. Res.*, **90**, 5629–5635.

Reed, R. J., 1966: Zonal wind behavior in the equatorial stratosphere and lower mesosphere. *J. Geophys. Res.*, **71**, 4223–4233.

Reed, R. J., W. J. Campbell, L. A. Rasmusson, and D. G. Rogers, 1961: Evidence of a downward-propagating annual wind reversal in the equatorial stratosphere. *J. Geophys. Res.*, **66**, 813–818.

Russell, P. B., M. P. McCormick, T. J. Swissler, W. P. Chu, J. M. Livingston, W. H. Fuller, J. M. Rosen, D. J. Hofmann, L. R. McMaster, D. C. Woods, and T. J. Pepin, 1981: Satellite and correlative measurements of the stratospheric aerosol. II, Comparison of measurements made by SAM II, dustsondes and an airborne lidar. *J. Atmos. Sci.*, **38**, 1295–1312.

Seidel, D. J., R. J. Ross, J. K. Angell, and G. C. Reid, 2001: Climatological characteristics of the tropical tropopause as revealed by radiosondes. *J. Geophys. Res.*, **106**, 7857–7878.

Seol, D.-I., and K. Yamazaki, 1998: QBO and Pinatubo signals in the mass flux at 100 hPa and stratospheric circulation. *Geophys. Res. Lett.*, **25**, 1641–1644.

Simkin, T., and R. S. Fiske, 1984: *Krakatau 1883, The Volcanic Eruption and Its Effects*. Smithsonian Institution Press, Washington, D.C., 464 pp.

Tegtmeier, S., J. Anstey, S. Davis, R. Dragani, Y. Harada, I. Ivanciu, R. P. Kedzierski, K. Krüger, B. Legras, C. Long, J. S. Wang, K. Wargan, and J. S. Wright, 2020: Temperature and tropopause characteristics from reanalysis data in the tropical tropopause layer. *Atmos. Chem. Phys.*, **20**, 753–770.

Thompson, D. W. J., and J. M. Wallace, 2001: Regional climate impacts of the Northern Hemisphere annular mode. *Science*, **293**, 85–89.

Trepte, C. R., 1993: *Tracer Transport in the Tropical Lower Stratosphere*. Ph.D. dissertation, University of Wisconsin–Madison, 160 pp. [Available at https://www.osti.gov/biblio/404799-tracer-transport-tropical-lower-stratosphere-ph-thesis.]

Trepte, C. R., and M. H. Hitchman, 1992: Tropical stratospheric circulation deduced from satellite aerosol data. *Nature*, **355**, 626–628.

Tuck, A. F., J. M. Russell III, and J. E. Harries, 1993: Stratospheric dryness: Antiphased desiccation over Micronesia and Antarctica. *Geophys. Res. Lett.*, **20**, 1227–1230.

Tucker, G. B., and J. M. Hopwood, 1968: The 26-month zonal wind oscillation in the lower stratosphere of the Southern Hemisphere. *J. Atmos. Sci.*, **25**, 293–298.

Veryard, R. G., and R. A. Ebdon, 1961: Fluctuations in tropical stratospheric winds. *Meteor. Mag.*, **90**, 125–143.

Virts, K. S., J. M. Wallace, Q. Fu, and T. P. Ackerman, 2010: Tropical tropopause transition layer cirrus as represented by CALIPSO lidar observations. *J. Atmos. Sci.*, **67**, 3113–3129.

Wallace, J. M., 1967: On the role of mean meridional motions in the biennial wind oscillation. *Quart. J. Roy. Meteor. Soc.*, **93**, 176–185.

Wallace, J. M., 1973: General circulation of the tropical lower stratosphere. *Rev. Geophys. Space Phys.*, **11**, 191–222.

Wallace, J. M., R. L. Panetta, and J. Estberg, 1993: Representation of the equatorial stratospheric quasi-biennial oscillation in EOF phase space. *J. Atmos. Sci.*, **50**,

1751–1762.

Wang, J., H.-M. Kim, and E. K. M. Chang, 2018: Interannual modulation of Northern Hemisphere winter storm tracks by the QBO. *Geophys. Res. Lett.*, **45**, 2786–2794.

Webster, P. J., and J. R. Holton, 1982: Cross-equatorial response to middle-latitude forcing in a zonally varying basic state. *J. Atmos. Sci.*, **39**, 722–733.

Winchester, S., 2003: *Krakatau - The Day The World Exploded: 27 August 1883*. Viking Press, 448 pp.

Yang, H., and K. K. Tung, 1996: Cross-isentropic stratosphere-troposphere exchange of mass and water vapor. *J. Geophys. Res.*, **101**, 9413–9423.

Yasunari, T., 1989: A possible link of the QBOs between the stratosphere, troposphere and sea surface temperature in the tropics. *J. Meteor. Soc. Japan*, **67**, 483–493.

Zhou, X. L., M. A. Geller, and M. H. Zhang, 2001: Tropical cold point tropopause characteristics derived from ECMWF reanalyses and soundings. *J. Climate*, **14**, 1823–1838.